공학석사 학위논문

Highly efficient copper (I) photosensitizer for photocatalytic hydrogen evolution from water

광촉매 물분해 수소생산을 위한 효율적인
구리 기반의 감광제에 대한 연구

2017년 2월

서울대학교 대학원

재료공학부

김 재 관

Highly efficient copper (I) photosensitizer for photocatalytic hydrogen evolution from water

A THESIS SUBMITTED IN PARTIAL FULFILLMENT OF
THE REQUESTMENTS FOR THE DEGREE OF MASTER
IN ENGINEERING AT THE GRADUATE SCHOOL OF
SEOUL NATIONAL UNIVERSITY

FEBURARY 2017

By

Jaekwan Kim

Supervisor

Prof. Soo Young Park

Abstract

Highly efficient copper (I) photosensitizer for photocatalytic hydrogen evolution from water

Jaekwan Kim

Department of Materials Science and Engineering

The Graduate School

Seoul National University

Recently the energy demand is surging as the polulation increases and the industrialization is accelerated. Fossil fuel which is the primary energy source is depletable and nuclear energy have a highly controversial topic about intrinsic dangers. Therefore, there is a rising interest in safe and eco-friendly energy which can replace scarce resources. Among the various alternative energies, hydrogen have the benefits of environment-friendly resource because the combustion by-product is only water. In addition, the specific energy of 120 to 142 MJ/kg is very high.

There are many ways to produce hydrogen. Reforming fossil fuels, which is the major way, causes environmental pollution. Electrolysis of water requires additional electric energy. To replace them, many researchers have been actively studying artificial photosynthesis that utilize infinite solar energy and water.

In this thesis, as a part of the artificial photosynthesis, I narrowed scope of study for photocatalytic water splitting to produce hydrogen. For the

photocatalytic reaction, development of an efficient photosensitizer is important. The photosensitizer is required to absorb visible light. The absorbed solar energy is converted into chemical energy. The most common photosensitizer materials are noble metal complexes such as $Ru(bpy)_3^{2+}$ or $Ir(ppy)_2(bpy)^+$. They are efficient, robust and able to absorb visible light. But the noble metals are inappropriate in point of practical view. For real application, they should be replaced to earth abundant metal complexes.

In chapter 2, I reported the design, synthesis, photophysical properties and hydrogen evolution application of efficient photosensitizers made from copper. To know how hydrogen evolution efficiencies vary according to functional group of ligand, I fine-tuned the properties of copper complex by changing size and electronic properties of ligands. Among them, a copper photosensitizer with bulky and electron donating triphenylamine moiety (Cu(TPA)) could absorb visible light largely because it can utilize ILCT (intralignad charge transfer) as well as MLCT (metal to ligand charge transfer). In addition, outstanding photophysical properties of Cu(TPA) such as high PLQY, long excited state lifetime and low non-radiative rate constant of Cu(TPA) were observed. Furthermore the bulky moiety of TPA enhanced the photostability. As a result, Cu(TPA) showed the highest efficiency for hydrogen evolution and the turnover number (TON) was 18974 for four days. The turnover frequency (TOF) of Cu(TPA) also increased in proportion to both of visible light absorption and free energy for electron transfer.

Keywords: Artificial photosynthesis, Water splitting, Photocatalytic hydrogen evolution, Metal complex, Copper (I) based photosensitizer
Student Number: 2015-20811

Contents

List of Abbreviations

ACT	Acetone
CuPS	Copper (I) photosensitizer
DCM	dichloromethane
DMA	*N*,*N*´-dimethylaniline
DMF	*N*,*N*´-dimethylformamide
DMSO	dimethylsulfoxide
EA	Ethyl acetate
h	hour
ILCT	Intraligand charge transfer
HOMO	highest occupied molecular orbital
LUMO	lowest unoccupied molecular orbital
NN	Diimine ligand
M	mole(s) per liter
MC	metal centered
MLCT	metal to ligand charge transfer
PP	Diphosphine ligand
PS	photosensitizer
SR	sacrificial reducing agent
TEA	triethylamine
THF	tetrahydrofuran
TLC	thin layer chromatography

TOF	turnover frequency
TON	turnover numbers
WRC	water reduction catalyst

List of Tables

List of Schemes

List of Figures

Chapter 1. Introduction

1.1 Artificial photosynthesis

Due to recent concern with regard to the depletion of fossil fuel and pollution of the environment, many are turning their attention to alternative source of energy. There are various kinds of alternative energy such as solar, wind, biomass and geothermal energies. Among them, researchers have recently studied about solar energy because sun light reaching the earth's surface is almost limitless, 1.2×10^5 TW of radiation of the earth.[1]

The solar energy can be converted into electrical energy by photovoltaic cells. It is the most commercialized but requires a battery system to store electricity. Another way is converting the solar energy into a storable fuel, not electricity. It is like photosynthesis which produces chemical energy sources such as carbohydrate. Photosynthesis generally occurs in green plants which have a green pigment called chlorophyll. After the chlorophyll in a photosystem absorbs sunlight, electrons are excited and transferred in the Calvin cycle. The water is oxidized and becomes oxygen at photosystem while carbon dioxide is reduced and becomes carbohydrate at the calvin cycle.[2]

The artificial photosynthesis mimics the original photosynthesis, so it includes the essential elements of photosynthesis: light harvesting unit, catalytic site and electron donor. Although the photosynthesis in nature makes oxygen and carbohydrate, the objective of artificial photosynthesis in this thesis

is to produce hydrogen. It is called water splitting. It is much easier than reduction of carbon dioxide to make carbohydrate because reduction of a water molecule to produce one hydrogen molecule requires only two electrons. Hydrogen is the most clean energy source, producing only water during combustion. In addition, it has high specific energy of about 120 MJ/kg. The value is more than twice that of natural gas. Therefore, the hydrogen production by water splitting is the promising solution of energy problems.

1.2 Photocatalytic hydrogen evolution

To produce hydrogen, there are some methods: reforming hydrocarbon from fossil fuel, electrolysis and photocatalysis from water. The current dominant method to produce hydrogen is reforming hydrocarbon.[3] Using fossil fuel as raw material is inconsistent with the purpose of alternative energy. A bigger problem is the environmental pollution such as CO_2 emission. Electrolysis is cleaner method than reforming. Because it supplies electricity to hydrogen evolution electrodes, the whole procedure is complex and consumes another electric energy.[4-8] Thus, the input energy for hydrogen production by electrolysis is more expensive. However, photocatalysis requires only water and solar energy so it is the most environmental-friendly and economical.

The components for producing hydrogen from water are photosensitizer (PS), water reduction catalyst (WRC) and sacrificial reagent (SR). PS absorbs visible light and converts it to chemical energy. WRC reduces protons to hydrogen and SR provides electrons to PS.[1] The photocatalytic hydrogen evolution begins with PS absorbing light. According to solar irradiance spectra, visible light comprises a large portion of sunlight arriving at the surface of the earth. Therefore PS should absorb visible light efficiently for real application. As the PS absorbs light, electrons in HOMO of the PS are excited to LUMO. Then, the PS becomes excited state PS^*. HOMO and LUMO of ground state of the PS are changed to two SOMO (singly occupied molecular orbital) of excited state PS^*: LSOMO (lowest singly occupied molecular orbital) and HSOMO

(highest singly occupied molecular orbital).[9] Because there are vacancies of electron in each SOMO after excitation, the mechanism of photocatalysis is divided into two ways (Figure 1.1). One way is that SR provides electrons to LSOMO of PS^*. The PS^* is reduced to PS^- and the process is called reductive quenching. The reduced PS^- transfers electrons to WRC. After the WRC gets two electrons and two protons from PS^- and water respectively, it can produce one hydrogen molecule. The other way is that electrons on HSOMO of PS^* are transferred to WRC beforehand. Then the PS^* is oxidized to PS^+. SR also transfers electrons to the vacancy of HOMO of oxidized PS^+ then it returns to ground state of PS. The procedure is oxidative quenching.

There are necessary conditions to make the photocatalytic cycle work well. First, PS should absorb visible light sufficiently. As the first step of the photocatalysis, it is the most important to make excited state PS^*. Second, long excited state lifetime is required because electrons are transferred by an efficient collision between chemical species before PS decays to the ground state. Third, both PS and WRC should be robust. There are many redox reactions and collision with each other. If the materials are not robust, the components are decomposed then the hydrogen evolution will be ceased. Fourth, the redox potential between PS, WRC and SR should be appropriate for electron transfer.

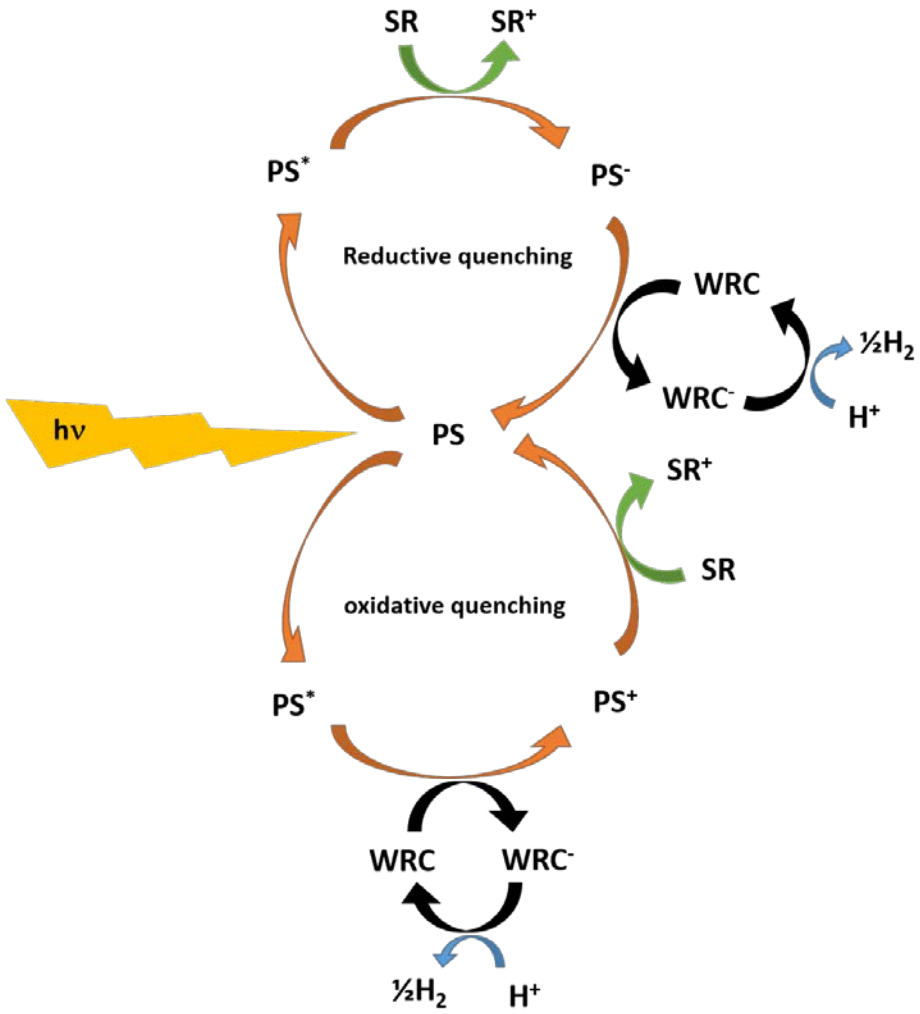

Figure 1.1 Mechanism of the photocatalytic hydrogen evolution

1.3 Metal complex for photocatalytic hydrogen evolution

As mentioned above, PS is very important in the photocatalytic hydrogen evolution system. PS should be able to absorb enough visible light, transfer electrons to WRC. Many kinds of materials for PS have been observed. Among them, heterogenous inorganic semiconductor materials have been studied thoroughly for a long time. Despite advantages of heterogeneous materials such as robustness and high activity, it is difficult to tune photophysical properties and catalytic activity because compositions of materials, particle size and shape are uncontrollable. However, in homogeneous system, transition metal complexes of organic materials can be controlled easily and precisely.

Transition metal complexes are used in various ways such as optoelectronic and photocatalytic applications like OLED, OPV and photocatalysis. The metal complexes consist of core transition metal and surrounding ligands. According to diverse combination of different metals and ligands, properties of complexes vary considerably. Many kinds of metal complexes have been developed and applied for photocatalytic hydrogen evolution (Figure 1.2).

Molecular orbitals of metal complexes consist of metal character and ligand character orbitals. There are many possible electron transitions between the orbitals. They can be classified to metel centered transition (MC), ligand centered transition (LC), metal-to-ligand charge transfer transition (MLCT) and ligand-to-metal charge transfer transition (LMCT). Each transition between the orbitals is dependent on kinds of metal and ligands. In molecular orbitals of

metal complexes, the d-orbitals are split in the ligand field. As changing coordination number and electronic properties of ligands, the gap between molecular orbital energies can be tuned finely. Thus, according to the energy states, the wavelength range of absorbed light and redox potentials are determined. If the energy of antibonding d-orbital of metal is high, MC and MLCT transition energies correspond to short wavelength.[1]

Among the various metal complexes, $Ru(bpy)_3^{2+}$ is the good example for PS of photocatalytic hydrogen evoluion. $Ru(bpy)_3^{2+}$ is the tranditional dye used in DSSC widely because it can absorb visible light through MLCT transition and its excited state lifetime is long enough to transfer electron to other chemical species.[10] Besides, 3rd row transition metal complexes such as iridium complex are better than ruthenium complex which is 2nd row transition metal complex.[11] This is because 3rd row transition metal complexes are more stable and able to control higher transition energy. Due to the advantages of heavy metal complexes, many researches about ruthenium or iridum complexes have been reported.[12-14]

Transition metal complexes are used as catalyst as well as PS. Because they have various oxidation states due to d-orbitals, they can be redox centers for active site of the catalyst.[15] For example, cobalt (II) in $Co(bpy)_3^{2+}$ as WRC can be reduced to cobalt (I) and also oxidized to cobalt (III).[16] On the other hand, some metal complex molecules such as platinum(II) and palladium(II) are decomposed during the photocatalysis and become colloid.[17] For example, K_2PtCl_4 is precursor of active colloidal catalyst. The colloidal platinum(0) is very active catalyst because of the low overpotential.

Molecular catalyst is important to study to reveal the artificial photosynthesis fundamentally. However, the low stability compared with heterogeneous materials is the fatal drawback. On the other hand, colloidal catalyst is very active but hard to be controlled. Therefore catalysts should be selected considering the strong and weak points.

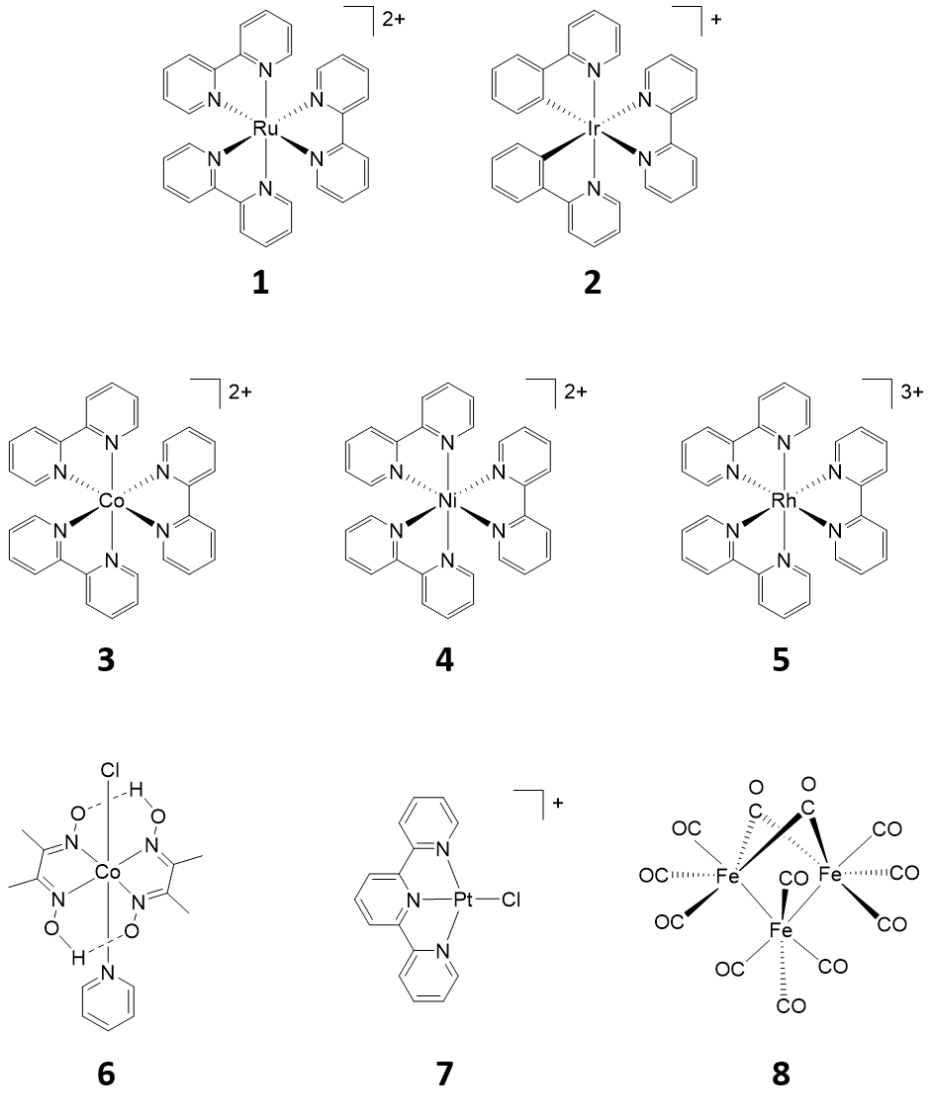

Figure 1.2 Examples of chemcial structure of transition metal complex for photocatalytic hydrogen evolution. Some of them are used as photosensitizer(**1-2**) and others are used as water reduction catalyst(**3-9**)

1.4 Copper(I) complex

There are many kinds of transition metal in the earth. Among them, people used copper for the longest time in real life as metal alloys, for example coins or weapons. Even though copper forms group 11 in the periodic table with gold and silver, it is the most commonly used among the three because of large abundance and low price.

Copper can have two oxidation state: copper (I) and copper (II).[18] In a copper (I) complex, electron configuration of Cu^{+} ion is $[Ar]3d^{10}$. Because of a full d subshell, copper (I) complexes do not have metal centered d-d transition contrary to other transition metal complexes (Figure 1.3). However, copper (II) complexes have d^{9} orbitals and suffer the d-d transitions of which the energy correspond to near-IR region. The low energy causes the non-radiative process.[19] Therefore copper (I) complexes are better for PS than copper (II) complexes.

There are many kinds of copper (I) complexes (Figure 1.4). They are studied a lot for optoelectronics such as OLED, LEC and DSSC.[20] First is tetrahedral coordinated copper (I) complexes. They are cationic complexes with neutral ligands such as diimine and diphosphine. They can be used as light emitting materials[21] because their emission performances are competitive. Especially, 2 of Figure 1.4 is known as TADF material. HOMO of the complex is located on the copper center and diphosphine ligand while LUMO is located on the diimine ligand. The electron locations of ground state and excited state

are different. In addition, they are soluble and absorb visible light. The complexes can be used as not only the light emitting materials, but also a PS of dye-sensitizied solar cells (DSSC).[22-26] Second and third are trigonal coordinated and polynuclear copper (I) complexes respectively. They have anionic ligands so the complexes are neutral. Because of neutrality of the complexes, they have been developed for application of OLED with various colors and emitting performance.[27-30]

The four-coordinated copper (I) complex prefers tetrahedral structure in ground state. When it is photoexcited, MLCT transition occurs. In the complex, the copper center is locally oxidized to copper (II). Because copper (II) prefers square planar, the structure of excited state of the complex is distorted. The structure difference between ground state and excited state causes non-radiative decay. It is important to hinder the distortion for highly emissive complex. To solve the problem, blocking moiety such as methyl group is attached at ligands toward copper center direction.

Copper (I) complexes with two ligands are homoleptic or heteroleptic. Homoleptic complexes, $[Cu(NN)_2]^+$, with same ligands have been studied for a long time (1 of Figure 1.4). However in recent heteroleptic complexes, $[Cu(NN)(PP)]^+$, with different ligands have got increasing attention because they are stronger emitters than homoleptic complexes (2 of Figure 1.4).[31] Diphosphine is more electron-withdrawing than diimine ligand so it tends to disfavor the electron transfer from copper center to diimine. It leads MLCT transition blue shift and oxidation potential higher. Therefore the bandgap becomes bigger. Because of energy gap law, emission of the heteroleptic

complex is enhanced compared with homoleptic complexes.[32]

The heteroleptic copper (I) complex can absorb visible light through MLCT transition. The excited state lifetime is long enough for electron transfer in microsecond timescale. In addition, they have proper redox potential. Therefore, recently, the complexes are developed for photocatalytic hydrogen evolution.

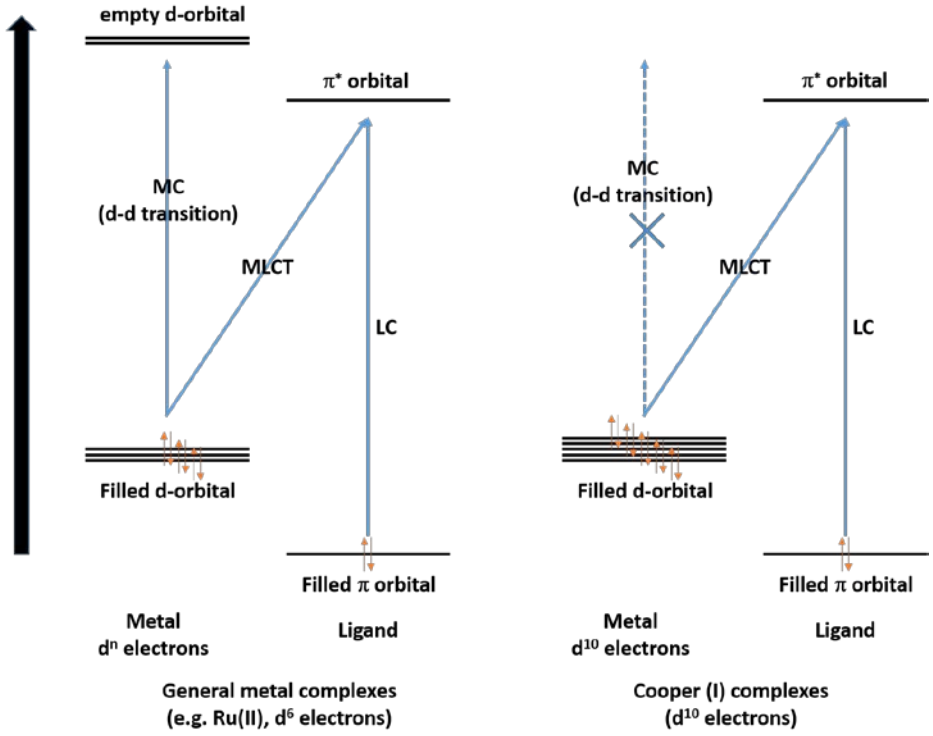

Figure 1.3 Electronic transition of general transition metal complexes and copper (I) complexes

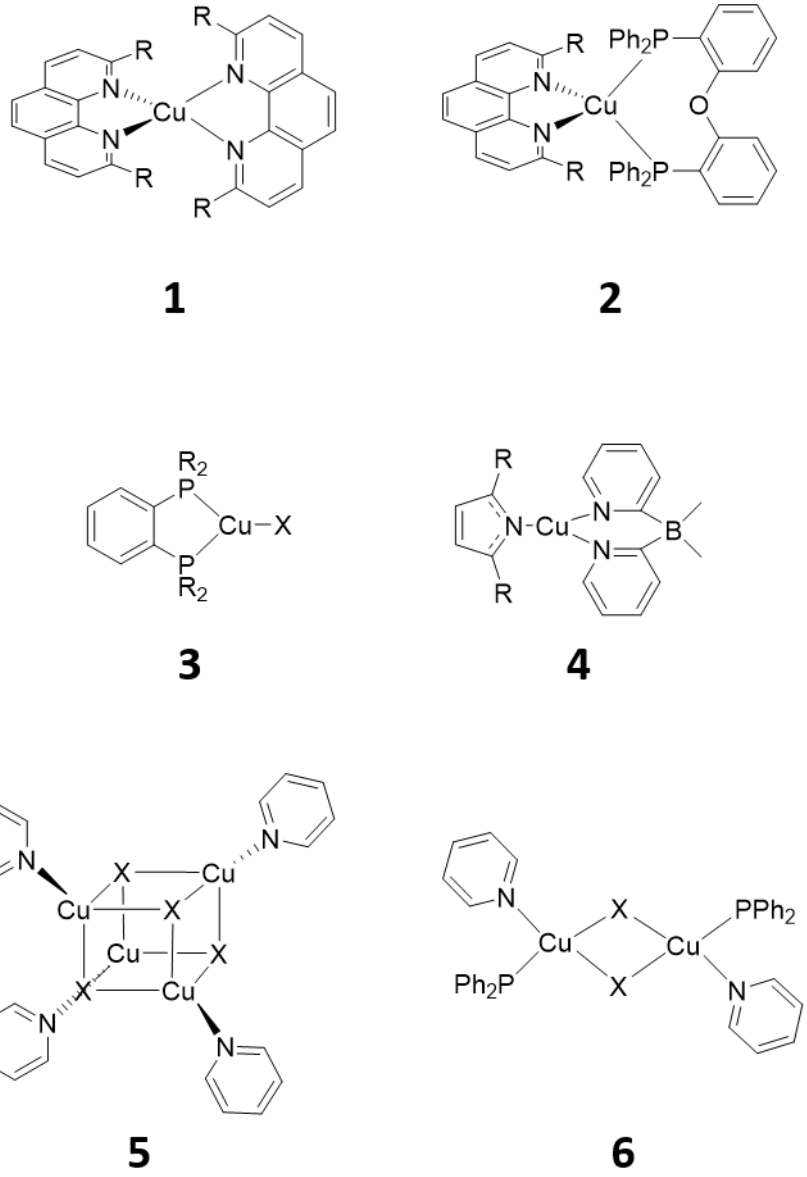

Figure 1.4 Examples of chemical structure for various copper complexes. Tetrahedral mononuclear complexes (**1-2**), trigonal mononuclear complexes (**3-4**), polynuclear complexes (**5-6**)

1.5 References

1. L. L. Tinker, N. D. McDaniel, S. Bernhard, *J. Mater. Chem.* **2009**, *19*, 3328.
2. Kim, J. H.; Lee, M.; Lee, J. S.; Park, C. B. *Angew. Chem.* **2012**, *51*, 517
3. J. M. Ogden, *Annu. Rev. Energy Environ.* **1999**, *24*, 227
4. A. J. Bard, M. A. Fox, *Acc, Chem, Res.* **1995**, *28*, 141
5. A. Currao, *Chimia.* **2007**, *61*, 815
6. P. D. Tran, L. H. Wong, J. Barber, J. S. C. Loo, *Energy & Environ. Sci.* **2012**, *5*, 5902
7. R. M. Navarro, M. C. Alvares-Galvan, J. A. Villoria de la Mano, S. M. Al-Zahrani, J. L. G. Fierro, *Energy & Environ. Sci.* **2010**, *3*, 1865
8. M. Kitano, M. Hara, *J. Mater. Chem.* **2010**, *20*, 627
9. L. L. Tinker, N. D. McDaniel, P. N. Curtin, C. K. Smith, M. J. Ireland, S. Bernhard, *Chem. Eur. J.* **2007**, *13*, 8726
10. Na, M. Wang, J. Pan, P. Zhang, B. Åkermark, L. Sun, *Inorg. Chem.* **2008**, *47*, 2805
11. J. I. Goldsmith, W. R. Hudson, M. S. Lowry, T. H. Anderson, S. Bernhard, *J. Am. Chem. Soc.* **2005**, *127*, 7502.
12. E. D. Cline, S. E. Adamson, S. Bernhard, *Inorg. Chem.*. **2008**, *47*, 10378
13. P. N. Curtin, L. L. Tinker, C. M. Burgess, E. D. Cline, S. Bernhard, *Inorg. Chem.*. **2009**, *48*, 10498
14. B. F. Disalle, S. Bernhard, *J. Am. Chem. Soc*. **2011**, *133*, 11819
15. W. T. Eckenhoff, R. Eisenberg, *Dalton transactions*. **2012**. *41*. 13004

16. V. Artero, M. Chavarot-Kerlidou, M. Fontecave, *Angew. Chem. Int. Ed*. **2011**, *50*, 7238

17. P. Lei, M. Hedlund, R. Lomoth, H. Rensmo, O. Johansson, L. Hammarstrom, *J. Am. Chem. Soc*, **2008**, *130*, 26

18. N. Armaroli, G. Accorsi, F. Cardinali, A. Listorti, *Top. Curr. Chem.* **2007**, *280*, 69

19. K. Kalyanasundaram, Photochemistry of polypyridine and porphyrin complexes, Academic Press, New York, **2002**

20. M. J. Leitl, D. M. Zink, A. Schinabeck, T. Baumann, D. Volz, H. Yersin, *Top. Curr. Chem.* **2016**, *374*, 25

21. R. D. Costa, E. Orti, H. J. Bolink, F. Monti, G. Accorsi, N. Armaroli, *Angew. Chem. Int. Ed*. **2012**, *51*, 8178

22. M. S. Lazorski, F. N. Castellano, *Polyhedron*, **2014**, *82*, 57

23. N. Robertson, *ChemsusChem*. **2008**, *1*, 977

24. B. Bozic-Weber, V. Chaurin, E. C. Constable, C. E. Housecroft, M. Meuwly, M. Neuburger, J. A. Rudd, E. Schonhofer, L. Siegfried, *Dalton Trans*. **2012**, *41*, 14157

25. A. H. Rendondo, E. C. Constable, C. E. Housecroft, *Chimia*, **2009**, *63*, 205

26. T. Bessho, E. C. Constable, M. Graetzel, A. H. Redondo, C. E. Housecroft, W. Kylberg, M. D. Nazeeruddin, M. Neuburger, S. Schaffner, *Chem.Commun*. **2008**, *32*. 3717

27. S. Igawa, M. Hashimoto, I. kawata, M. Yashima, M. Hoshino, M. Osawa, *J. Mater, Chem. C*. **2013**, *1*, 542

28. M. Osawa, *Chem. Commun*. **2014**, *50*, 1801

29. K. J. Lotito, J. C. Peters, *Chem. Commun*. **2010**, *46*, 3690

30. J. C. Deaton, S. C. Switalski, D. Y. Kondakov, R. H. Young, T. D. Pawlik, D. J. Giesen, S. B. Harkins, A. J. M. Miller, S. F. Mickenberg, J. C. Peters, *J. Am. Chem. Soc*. **2010**, *132*, 9499

31. A. Barbieri, G. Accorsi, N. Armaroli, *Chem. Commun.* **2008**, *19*, 2186

32. S, -M, Kuang, D. G. Cuttell, D. R. McMillin, P. E. Fanwick, R. A. Walton, *Inorg. Chem.* **2002**, *41*, 3313

Chapter 2. Efficient photocatalytic hydrogen evolution from water using copper(I) photosensitizer containing electron donating moiety

2.1 Introduction

In photocatalytic hydrogen evolution system, the process starts from the photoexcitation of a PS.[1] It is important to develop the PS to absorb the light and transfer electrons to catalyst efficiently. The requirements of efficient PS are high absorbance of visible light, long excited state lifetime, low non-radiative decay, appropriate redox potential and high stability.

The noble metal complexes such as $Ru(bpy)_3^{2+}$ meet the requirements of PS so well that they have been used widely in this system. Although they have been studied deeply for a long time, the high price and the scarcity of noble metals have to face the problems for real applications. Especially, in the general case of this system, the number of photosensitizers is 1 to 10^3 times more than that of catalysts to transfer electrons. From an economic point of view, the photosensitizers should be made of cheap materials.

To overcome the problem, there have been many attempts to replace the noble metal complexes with pure organic materials or earth abundant metal

complexes. However, organic dyes are insufficient for PS because of short excited state lifetime and susceptibility to photobleaching. Instead, heteroleptic copper (I) complexes with diimine and diphosphine ligands are known that they have long excited state lifetime and high PLQY. Therefore it was possible to use the copper (I) complexes as PS in photocatalytic hydrogen evolution.

Castellano group first reported a homoleptic copper (I) complex with two phenanthroline ligands (Figure 2.1)[12]. Then Beller gruop reported heteroleptic copper (I) complexes and recorded high TON of 1330 in homogeneous system. However the value was not comparable to replace the noble metal based PSs yet[13]. Their strategies were introducing alkyl chains on phenanthroline ligand toward the copper center to prevent the deactivation physically. The chains were methyl, n-butyl, s-butyl, i-butyl, i-propyl and n-hexyl group. s-butyl and i-propyl chains could reduce the non-radiative decay efficiently thus extend excited state lifetime. The strategy was good for enhancing the efficiency however n-hexyl and i-butyl chains rather lowered efficiency compared with methyl substituent. Therefore, there was no certain rule to inhibit the non-radiative decay by using alkyl chain. Moreover, alkyl chains cannot affect the electronic characteristics of the complexes. If the substituents of phenanthroline toward copper center are much bulkier like aromatic rings, a diphosphine ligand cannot coordinate copper center to make a heteroleptic complex by steric hindrance[14].

Therefore, it is required to develop new strategy to inhibit the decay without attaching substituents toward copper center. I tried to tune the properties of the complexes by changing the substituents with different size and electronic

character at periphery of the phenanthroline ligand and fixed methyl groups toward the copper center.

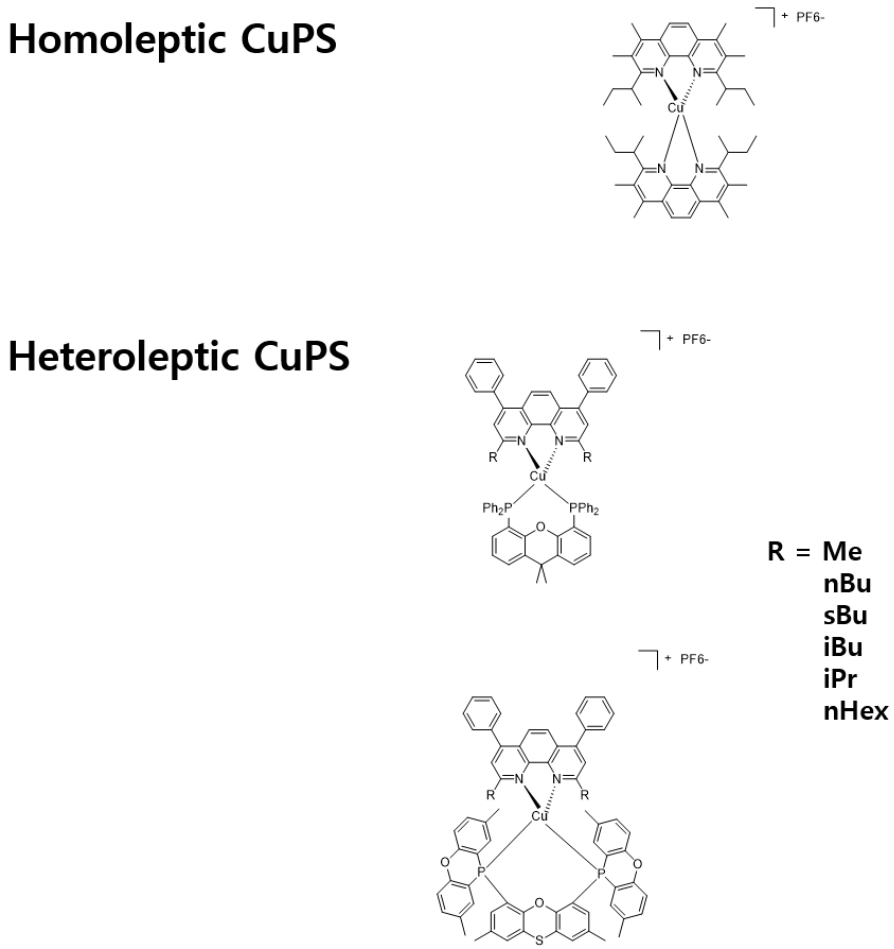

Figure 2.1. Reported copper (I) PSs for photocatalytic hydrogen evolution[12,13]

2.2 Experimental section

Material design

To adjust properties of copper (I) complex, substituents of the ligand should be modified. The influence of electron donating or withdrawing character of ligands is substantial for the photocatalytic activity. Some studies, in particular, showed that metal complexes with electron donating moiety has high molar extinction coefficient.

High absorbance of visible light of the PS is important. The more photons are absorbed by PS, the faster the hydrogen is evolved.[2] For visible light absorption, metal complexes such as ruthenium (II) or iridium (III) complexes have been used because the range of their MLCT absorption band extends above 400 nm. However, the extinction coefficient of MLCT was still low to utilize. Many groups studying DSSC using ruthenium (II) complexes have tried to tune the ligand to increase the extinction coefficient.[3-7] One of trials was introducing an electron donor to the ligand. Incorportion of electron delocalization donor antenna substituents can increase the harvesting abilities.[8-10] There are many donor moieties but triphenylamine (TPA) has been widely used because of their structural versatility, low cost and high extinction coefficient.[11] The absorption bands were ascribed to intraligand charge-transfer (ILCT) transitions, not MLCT.

In addition, it was demonstrated that bulky moiety increases the stability of the complex and enhances the photocatalytic activity. Therefore, the

substituents can be designed with different size and electronic feature at periphery of the phenanthroline ligand, not toward copper center to make diphosphine ligand to coordinate the copper.

I described on the use of TPA groups as electron donating and bulky moiety to increase visible light absorption and to circumvent the non-radiative deactivation. In addition to TPA, other ligands with various functional group were designed. DMA and BZN ligands were used to compare the effect of electronic characters. Each substituent of the ligands were dimethylaniline as another electron donating moiety and benzonitrile as electron withdrawing moiety respectively. I also explored the relationship between the size of substituents and designed TPS (triphenylsilane), BCP (bathocuproine, 2,9-dimethyl-4,7-diphenyl-1,10-phenanthroline) and dmphen (2,9-dimethyl-1,10-phenanthroline) ligands. Tetraphenylsilane was chosen as a bulky moiety to minimize electronic effect compared with BCP. As a diphosphine ligand, xantphos (4,5-Bis(diphenylphosphino)-9,9-dimethylxanthene) was selected because of its rigid structure.

Scheme 2.1 illustrates the chemical structures of copper (I) complexes investigated in this work. All copper (I) complexes with the ligands were synthesized according to standard procedures. (Scheme 2.2)

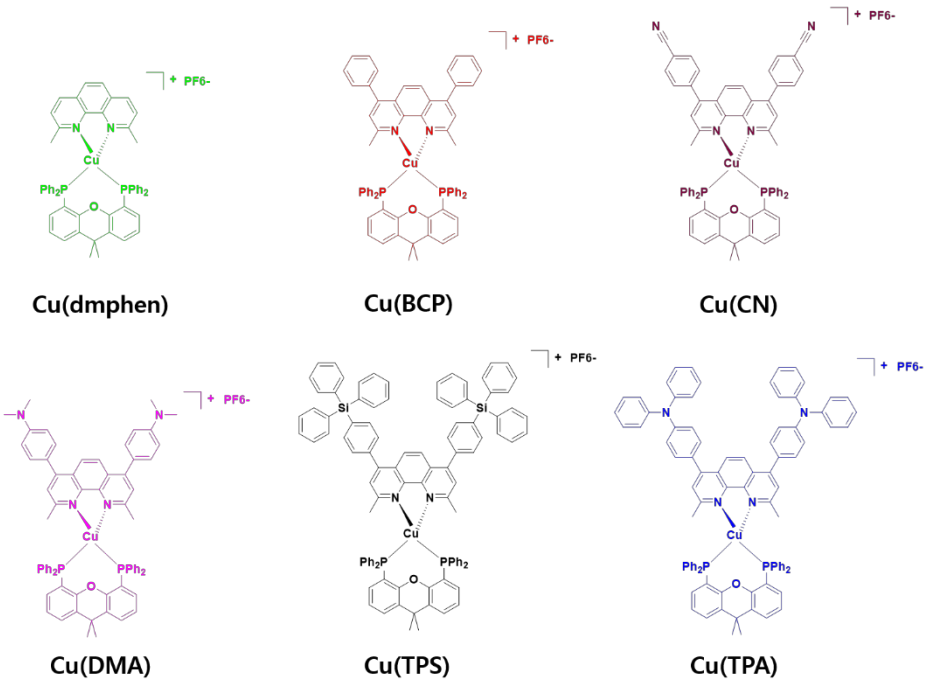

Scheme 2.1. Chemical structures of target materials.

General Methods

Commercially available chemicals were purchased from Sigma-Aldrich, Alfa Aesar and TCI. All glassware and magnetic stirring bar were cleaned and dried in an oven before use. Reactions were monitored using thin layer chromatography (TLC). Commercial TLC plates (silica gel 254, Merck Co.) were developed and the spots were visualized under UV light at 254 or 365 nm. Silica gel column chromatography was performed with silica gel 60 G (particle size 5-40 μm, Merck Co.). 1H NMR spectra were collected with a Bruker AVANCE-300 NMR spectrometer. Chemical shifts (δ) are recorded in ppm and referenced to TMS. The peak splitting is abbreviated as follows : s = singlet; d = doublet; t = triplet; m = multiplet and the coupling constants (*J*) are in Hz. High-resolution mass spectrometry (HRMS) spectra were recorded on a JMS-700 MStation (JEOL).

Synthesis

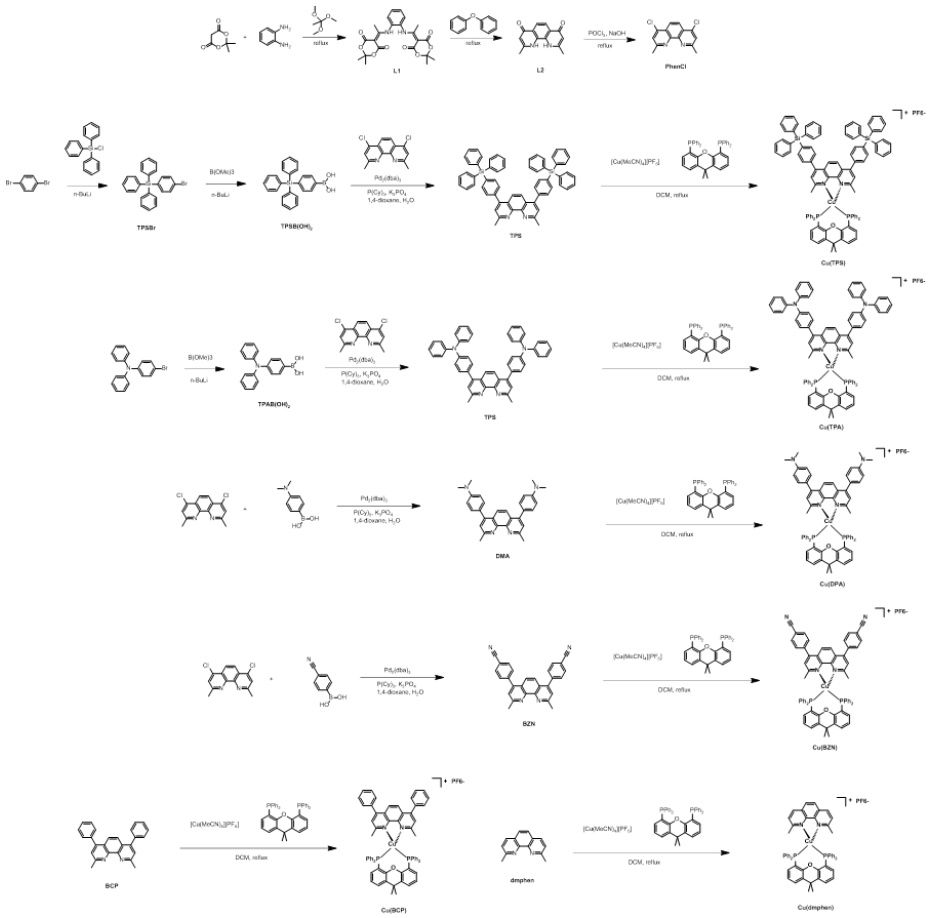

Scheme 2.2. Synthesis of target materials and ligands

5,5’-((1,2-phenylenebis(azanediyl))bis(ethan-1-yl-1-ylidene))bis(2,2-diethyl-1,3-dioxane-4,6-dione) (L1)[15]

Meldrum’s acid (4 g, 27.75 mmol, 2.2 equiv) and trimethyl orthoformate (100 mL) were stirred and refluxed for 15 min in a round bottom flask. The solution was cooled and o-phenylenediamine (1.364 g, 12.62 mmol 1 equiv) was added

portionwise. The mixture was refluxed again for 2 h. After reflux, it was cooled at r.t. and stirred overnight. The resulting solid was filtered and washed with ether. The solid is dried without further purification. Yield : 2.3992 g (42.79%); ^{1}H NMR(300 MHz, $CDCl_3$) δ 12.80 (s, 2H), 7.50 (dd, J = 6, 3 Hz, 2H), 7.36 (dd, J = 6, 4 Hz, 2H), 2.55 (s, 6H), 1.72 (s, 12H); HRMS m/z 444.16094 ([M+H$^+$]; calcd : 444.16054)

2,9-dimethyl-1,10-phenanthroline-4,7(1H,10H)-dione (L2)[15]

Diphenyl ether (500 mL) was heated at 200 °C in a round bottom flask. L1 (20 g, 45 mmol) was added portionwise. The solution was refluxed for 30 min. After cooling to 70 °C, a formed precipitate was filtered and washed with aceton, n-hexane and ether. The solid are dried without further purification. Yield : 11.9774 g (42.73%); ^{1}H NMR (300 MHz, NaOD in D_2O) δ 7.58 (s, 2H), 6.20 (s, 2H), 2.23 (s, 6H); HRMS m/z 241.09771 ([M+H$^+$]; calcd : 241.09715)

4,7-dichloro-2,9-dimethyl-1,10-phenanthroline (PhenCl)[15]

In a round bottom flask were added phosphoryl chloride (250 mL) and L2 (2.8 g, 11.65 mmol). The solution was refluxed at 90 °C for 4 h. After cooling the solution, it was slowly poured into 1 L of ice water. While it was stirred, chloroform was added to make organic layer. Sodium hydroxide powder was added very carefully until the pH of solution became 13-14. The organic layer are extracted and concentrated. The crude are purified using a silica gel column chromatography with mixed solution of MeOH:DCM 1:20 v/v as eluents. Yield : 3 g (92.89%); ^{1}H NMR (300 MHz, $CDCl_3$) δ 8.23 (s, 2H), 7.64 (s, 2H),

2.94 (s, 6H); HRMS m/z 277.03003 ([M+H$^+$]; calcd : 277.02938)

(4-bromophenyl)triphenylsilane (TPSBr)[14]

In a flame-dried round bottom flask was added p-dibromobenzene (4.8 g, 20.3 mmol, 1 equiv) in anhydrous ether (40 mL). The solution was coold down to -78 ℃ . 8.14 mL of n-BuLi (2.5 M in hexane, 20.3 mmol) was added dropwise slowly. After strring for 1 h, the reaction was warmed to r.t. and stirred for 1 h again. The, triphenylsilylchloride (5 g, 17.0 mmol) was delivered dripwise via syringe. After 2 h strring, the solution was poured into 80mL of water and the crude product was extracted with ether. Reprecipitate was filtered and washed with THF and MeOH. Yield : 5.273 g (74.86%); ^{1}H NMR (300 MHz, $CDCl_3$) δ 7.55 (m, 3H), 7.52 (m, 4H), 7.50 (m, 1H), 7.35-7.46 (m, 11H)

(4-(triphenylsilyl)phenyl)boronic acid (TPSB(OH)$_2$)[16]

In a flame-dried round bottom flask were added TPSBr (5.271 g, 12.7 mmol, 1 equiv) in anhydrous THF (60 mL). The solution was coold down to -78 ℃ . 8.12 mL of n-BuLi (2.5 M in hexane, 20.3 mmol, 1.6 equiv) was added dropwise slowly. After strring for 1 h, trimethyl borate(2.1 g, 20.3 mmol, 1.6 equiv) was added dropwise for 10 min. Then, the reaction was warmed to r.t. and stirred for 2 h again. The solution was poured into water and acidified with aqueous 1 M HCl. The crude product was extracted with EtOAc and purified using a silica column chromatography with a mixed solution of n-Hexane:EtOAc = 9:1. Yield : 2.2822 g (47.3%); ^{1}H NMR (300 MHz, $CDCl_3$) δ 8.20 (d, J = 12 Hz, 2H), 7.71 (d, J = 7 Hz, 2H), 7.54-7.63 (m, 7H), 7.35-7.47

(m, 10H)

(4-(diphenylamino)phenyl)boronic acid (TPAB$(OH)_2$)

In a flame-dried round bottom flask were added 4-bromotriphenylamine (2.945 g, 9 mmol, 1 equiv) in anhydrous THF (80 mL). The solution was coold down to -78 °C . 5.7 mL of n-BuLi (2.5 M in hexane, 14.4 mmol, 1.2 equiv) was added dropwise slowly. After strring for 3 h, trimethyl borate (4.1 mL, 36 mmol, 3.6 equiv) was added dropwise slowly. After stirring for 2 h more, the reaction was warmed to r.t. To the solution were added 60 mL of aqueous HCl (1 M) to acidify and stirred 3 h. The solution was poured into water and extracted with DCM and purified using a silica column chromatography with a mixed solution of DCM:ACT = 10:1. Yield : 1.3 g (49.96%); ^{1}H NMR (300 MHz, DMSO) δ 7.86 (s, 2H), 7.68 (d, J = 9 Hz, 2H), 7.31 (t, J = 9 Hz, 4H), 7.03(m, 6H), 6.89 (d, J = 9 Hz, 2H); HRMS m/z 290.13479 ([M+H^+]; calcd : 290.13469)

General procedure for NN ligand

PhenCl (1 equiv), boronic acid (2.125 equiv), tricyclohexylphosphine (0.046 equiv), and potassium phosphate (2.125 equiv) were dissolved in mixed solution of 1,4-dioxane:H_2O 3:1 v/v. The mixture was heated at 70 °C then N_2 purged 1,4-dioxane solution of tris(dibenzylidenacetone)dipalladium(0) (0.02 equiv) was added. The solution was reflux overnight. The crude mixture was poured into DCM and H_2O then extracted into the organic layer. The organic layer was concentrated and purified using a silica gel column chromathgraphy with mixed solution of MeOH:DCM to give a powder.

2,9-dimethyl-4,7-bis(4-(triphenylsilyl)phenyl)-1,10-phenanthroline (TPSphen)

PhenCl 300mg (1.08 mmol) used, Yield: 844 mg (89%). ^{1}H NMR (300 MHz, $CDCl_3$) δ 7.81 (s, 2H), 7.73 (s, 2H), 7.70 (s, 2H), 7.64 (m, 6H), 7.61 (m, 6H), 7.54 (s, 2H), 7.52 (s, 2H), 7.38-7.50 (m, 20H); HRMS m/z 877.34364 ([M+H$^+$]; calcd : 877.34288)

4,4'-(2,9-dimethyl-1,10-phenanthroline-4,7-diyl)bis(N,N-diphenylaniline) (TPAphen)

PhenCl 360.8 mg (1.3 mmol) used, Yield: 530 mg (58.67%). ^{1}H NMR (300 MHz, $CDCl_3$) δ 7.91 (s, 2H), 7.46 (s, 2H), 7.41 (d, J = 9 Hz, 4H), 7.28-7.34 (m, 8H), 7.17-7.21 (m, 12H), 7.08 (m, 4H), 2.98 (s, 6H); HRMS m/z 695.31712 ([M+H$^+$]; calcd : 695.31692)

4,4'-(2,9-dimethyl-1,10-phenanthroline-4,7-diyl)bis(N,N-dimethylaniline) (DMAphen)

PhenCl 237.13 mg (0.856 mmol) used, Yield: 232.7 mg (60.9%). ^{1}H NMR (300 MHz, $CDCl_3$) δ 7.88 (s, 2H), 7.45 (d, J = 9 Hz, 4H), 7.41 (s, 2H), 6.86 (d, J = 9 Hz, 4H), 3.05 (s, 12H), 2.96 (s, 6H); HRMS m/z 447.25482 ([M+H$^+$]; calcd : 447.25432)

4,4'-(2,9-dimethyl-1,10-phenanthroline-4,7-diyl)dibenzonitrile (BZNphen)

PhenCl 300mg (1.08 mmol) used, Yield: 363.5 mg (82.0%). ^{1}H NMR (300 MHz, $CDCl_3$) δ 7.84 (d, J = 8 Hz, 4H), 7.65 (d, J = 9 Hz, 6H), 7.45 (s, 2H),

3.02(s, 6H); HRMS m/z 411.16081 ([M+H$^+$]; calcd : 411.16042)

General procedure for [Cu(NN)(PP)]$^+$PF$_6^-$ (Cu(NN))

[Cu(NN)(PP)]$^+$PF$_6^-$ was synthesized according to the literature procedure.[17] [Cu(MeCN)$_4$]$^+$PF$_6^-$ (1 eq) and 4,5-Bis(diphenylphosphino)-9,9-dimethylxanthene(xantphos) (1 eq) were dissolved in 10mL anhydrous DCM. The mixture was stirred at 40 °C reflux overnight under Ar atmosphere. Then the mixture is cooled at room tempeuratre and the phenanthorline ligand solution is added with minimum amount of DCM. After reflux more 6h, the crude product was cooled to room temperature and put dropwise into n-hexane to precipitate the product. Resulting product was washed with n-hexane, filtered, and dried overnight in vacuum oven at 60 °C. Dried solid was purified using a silica gel column chromatography with mixed solution of MeOH:DCM 1:20 v/v as eluents and recrystaliztion in a DCN/n-hexane.

[Cu(2,9-dimethyl-4,7-bis(4-(triphenylsilyl)phenyl)-1,10-phenanthroline)(xantphos)] $^+$PF$_6^-$ (Cu(TPS))

[Cu(MeCN)$_4$]PF$_6^-$ 128.38 mg (0.344 mmol) used, yellow solid, Yield: 483 mg (84 %). ^{1}H NMR (300 MHz, CDCl$_3$) δ 7.80 (s, 2H), 7.76 (d, J = 9 Hz, 4H), 7.59-7.67 (m, 14H), 7.39-7.50 (m, 24H), 7.18-7.23 (8, 2H), 7.02-7.11 (m, 14H), 6.95 (m, 2H), 2.33 (s, 6H), 1.75 (s, 6H); ^{13}C NMR (500 MHz, CDCl$_3$) δ 158.13, 155.24, 155.19, 155.13, 150.06, 143.83, 137.60, 137.07, 136.59, 133.97, 133.73, 133.26, 133.20, 133.14, 131.73, 131.60, 130.51, 130.18, 130.13, 129.01, 128.85,

128.82, 128.78, 128.29, 127.85, 125.70, 125.64, 125.59, 123.76, 121.68, 121.58, 121.48, 36.31, 28.82, 27.60 ; HRMS m/z 1517.4571 ([M-PF_6^-]+; calcd : 1517.4580)

[Cu(4,4'-(2,9-dimethyl-1,10-phenanthroline-4,7-diyl)bis(N,N-diphenylaniline))(xantphos)] $^+PF_6^-$ (Cu(TPA))

$[Cu(MeCN)_4]PF_6^-$ 96.3 mg (0.258 mmol) used, yellow solid, Yield: 271.5 mg (71 %). ^{1}H NMR (300 MHz, $CDCl_3$) δ 7.93 (s, 2H), 7.66 (d, J = 6 Hz, 2H), 7.42 (s, 2H), 7.30-7.35 (m, 12H), 7.17-7.25 (m, 18H), 7.02-7.14 (m, 20H), 6.95 (m, 2H), 2.30 (s, 6H), 1.75 (s, 6H)); ^{13}C NMR (500 MHz, $CDCl_3$) δ 157.78, 155.20, 155.15, 149.88, 149.25, 147.19, 144.00, 133.92, 133.21, 133.15, 133.10, 131.75, 131.62, 131.49, 130.63, 130.44, 130.09, 129.73, 129.18, 128.76, 128.73, 128.73, 128.71, 127.74, 125.67, 125.54, 125.44, 125.14, 124.14, 123.59, 122.26, 121.65, 36.25, 28.73, 27.51; HRMS m/z 1335.4332 ([M-PF_6^-]+; calcd : 1335.4321)

[Cu(2,9-dimethyl-4,7-diphenyl-1,10-phenanthroline)(xantphos)] $^+PF_6^-$ (Cu(BCP))

$[Cu(MeCN)_4]PF_6^-$ 128.38 mg (0.344mmol) used, yellow solid, Yield: 327.6 mg (83 %). ^{1}H NMR (300 MHz, $CDCl_3$) δ 7.78 (s, 2H), 7.67 (d, J = 9Hz, 2H), 7.55 (m, 6H), 7.46 (m, 6H), 7.19-7.32 (m, 4H), 7.09 (m, 14H), 6.98 (m, 2H), 2.33 (s, 6H), 1.76 (s, 6H) ; ^{13}C NMR (500 MHz, $CDCl_3$) δ 158.02, 155.29, 155.23, 155.18, 150.39, 143.82, 136.54, 133.98, 133.28, 133.22, 133.16, 131.77, 131.64, 131.51, 130.55, 130.13, 129.63, 129.59, 129.25, 128.87, 128.83, 128.80, 127.79, 125.84, 125.64 125.62, 123.79, 121.79, 121.69, 121.59, 36.33, 28.79, 27.59;

HRMS m/z 1001.2849 ([M-PF_6^-]+; calcd : 1001.2851)

[Cu(4,4'-(2,9-dimethyl-1,10-phenanthroline-4,7-diyl)bis(N,N-dimethylaniline))(xantphos)] $^+PF_6^-$ (Cu(DMA))

$[Cu(MeCN)_4]PF_6^-$ 128.38 mg (0.344mmol) used, yellow solid, Yield: 305.4 mg (72 %). ^{1}H NMR (300 MHz, $CDCl_3$) δ 7.92 (s, 2H), 7.65 (d, J = 9 Hz, 2H), 7.36-7.41 (m, 6H), 7.17-7.23 (m, 6H), 7.02-7.12 (m, 16H), 6.93 (m, 2H), 6.87 (d, J = 9 Hz, 4H), 3.07 (s, 12H), 2.27 (s, 6H), 1.69 (s, 6H)); ^{13}C NMR (500 MHz, $CDCl_3$) δ 157.28, 155.17, 151.14, 150.49, 144.16, 133.89, 133.21, 133.16, 133.10, 131.83, 131.70, 131.57, 130.83, 130.41, 130.03, 128.72, 128.68, 128.65, 127.60, 125.72, 125.46, 124.62, 123.56, 121.80, 112.33, 40.40, 36.22, 28.67, 27.49; HRMS m/z 1087.3687 ([M-PF_6^-]+; calcd : 1087.3695)

[Cu(4,4'-(2,9-dimethyl-1,10-phenanthroline-4,7-diyl)dibenzonitrile)(xantphos)] $^+PF_6^-$ (Cu(BZN))

$[Cu(MeCN)_4]PF_6^-$ 128.38 mg (0.344 mmol) used, yellow solid, Yield: 340.5 mg (82.6 %). ^{1}H NMR (300 MHz, $CDCl_3$) δ 7.86 (m, 4H), 7.67 (m, 8H), 7.48 (s, 2H), 7.19-7.23 (m, 6H), 7.06-7.08 (m, 16H), 6.96 (m, 2H), 2.35 (s, 6H), 1.75 (s, 6H); ^{13}C NMR (500 MHz, $CDCl_3$) δ 158.41, 155.13, 155.07, 155.02, 148.05, 143.59, 140.93, 133.85, 133.11, 133.05, 133.00, 132.90, 131.47, 131.33, 131.20, 130.63, 130.45, 130.21, 128.81, 128.78, 128.74, 127.75, 125.66, 125.57, 125.21, 123.64, 121.53, 121.43, 121.33, 118.44, 113.16, 36.19, 28.69, 27.56 ; HRMS m/z 1051.2771 ([M-PF_6^-]+; calcd : 1051.2756)

[Cu(2,9-dimethyl-1,10-phenanthroline)(xantphos)] $^{+}PF_6^{-}$ (Cu(dmphen))

$[Cu(MeCN)_4]PF_6^{-}$ 128.38 mg (0.344 mmol) used, pale yellow solid, Yield: 256.8 mg (75 %). ^{1}H NMR (300 MHz, $CDCl_3$) δ 8.33 (d, J = 9 Hz, 2H), 7.82 (s, 2H), 7.64 (d, J = 9 Hz, 2H), 7.52 (d, J = 6 Hz, 2H), 7.21 (m, 6H), 7.01 (m, 16H), 6.89 (m, 2H), 2.24 (s, 6H), 1.74 (s, 6H)); ^{13}C NMR (500 MHz, $CDCl_3$) δ 158.58, 155.30, 143.01, 138.20, 133.97, 133.17, 133.11, 133.04, 131.69, 131.55, 131.42, 130.56, 130.17, 128.85, 128.82, 128.78, 128.00, 127.58, 126.30, 125.59, 125.45, 121.93, 121.83, 121.73, 36.32, 28.66, 27.31; HRMS m/z 849.2240 ($[M-PF_6^{-}]+$; calcd : 849.2225)

Hydrogen Evolution Experiment

- Closed vessel system

Samples for photocatalytic hydrogen evolution were prepared by adding PS and WRC in the solution of THF:H_2O:TEA 8:2:2 v/v/v into a 40 mL air-tight vial equipped with a teflon septum. The sample in the light-shielded vial was bubbled for 15 min by Ar with 1% CH_4 as internal standard. Then the vial was irradiated with 300 W Xe lamp with 400 nm cutoff filter to eliminate ultraviolet light. The gas (200 μL) in the headspace above the sample was extracted using a Hamilton Lurelock-type syringe then injected into a gas chromatography (Agilent 7890A) equipped with metal packed GC column (60/80 molecular sieve 5A support). The amount of hydrogen evolved was calculated with the integrated area of hydrogen signal calibrated by the integrated area of CH_4 signal.

- Continuous flow system

Samples for photocatalytic hydrogen evolution were prepared by adding PS and WRC in the solution of DMF:H_2O:DMA 8:2:2 v/v/v into a 20 mL air-tight vial equipped with a teflon septum. The sample was stirred by magnetic stirring bar and gas in the samples were continuously exchanged with constant flow of Ar (5 sccm). Then the vial was irradiated with 300 W Xe lamp with 400 nm cutoff filter to eliminate ultraviolet light. The vent gas from the vial was introduced to automated 6-way valve system with 2 mL sampling loop and analyzed with the gas chromatography (Scheme 2.3). The amount of hydrogen evolved was calculated with the integrated area of 1000 ppm hydrogen in Ar signal.

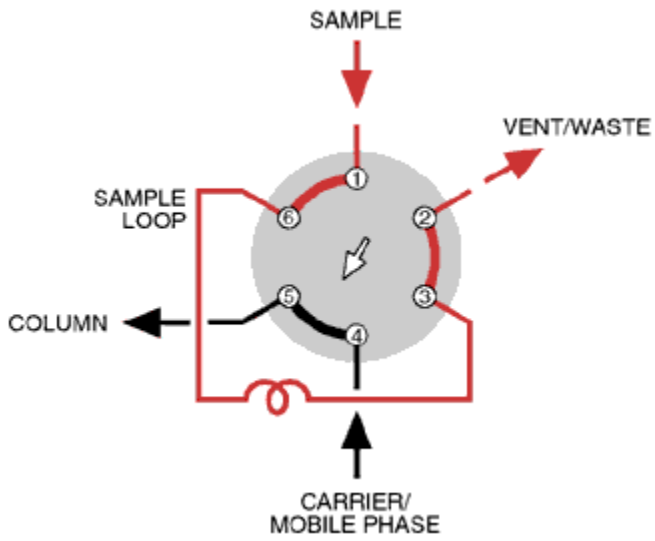

Scheme 2.3. Automated 6-way valve system[18]

Mesaurement

Absorption spectra were recorded using a Shimadzu UV-1650-PC from 250 to 900 nm. Steady-state photoluminescence (PL) spectra were obtained with a PTI QuantaMaster 40 spectrofluorometer in the range of 400-800 nm. Photoluminescence decay traces were recorded using time-correlated single photon counting (TCSPC) technique with a PicoQuant NanoHarp 250 instrument equipped with a LDH-P-C-375 pulsed diode laser (377 nm; fwhm < 80 ps). Data analyses were performed using a PicoQuant Fluofit software. The quality of the fit was assessed by the reduced χ^2 value and visual inspection of the weighed residuals. Cyclic voltammetric experiments were carried out with a Princeton Applied Research Potentiostat/Galvanostat Model 273A using three-electrode cell assemblies including a glassy-carbon working electrode, a platinum wire counter electrode, and a Ag/Ag^+ reference electrode. After Ar saturation in a one compartment cell, measurements were carried out in acetonitrile solution with tetrabutylammonium hexafluorophosphate (TBAHFP) as a supporting electrolyte at a scan rate of 100 mV/s.

DFT calculation

Calculations of the electronic ground states were carried out using B3LYP density functional theory together with the 6-31G basis set for C, H, N, O, and S atoms and the "double-ζ" quality basis set consisting of Hay and Wadt's effective core potentials (LANL2DZ)23,24 was employed for Ir atom. All

calculations were carried out using Gaussian 09.

2.3 Result and discussion

As illustrated in scheme 2.2 above, all intermediates and copper (I) complexes were synthesized successfully according to the literature methods. The assignment of intermediates were ^{1}H NMR and final products were analyzed by ^{1}H NMR, ^{13}C NMR and HRMS.

First, I measured the UV/Vis absorption spectra of the complexes. All of complexes showed absorption bands at two regions in common. The one was ligand π- π^{*} transition band of high molar extinction coefficient around 300 nm in ultraviolet region. The other was MLCT transition band of low molar extinction coefficient around 400 nm. Because the MLCT band extends toward above 400 nm, the hydrogen evolution experiments can utilize visible light region.

Cu(TPA) and Cu(DMA) have electron donating moieties, TPA and DMA, respectively. They showed dramatically large absorption in visible light region compared with other complexes (Figure 2.2). The extinction coefficient of the two complexes were 34,700 $M^{-1}cm^{-1}$ and 29,400 $M^{-1}cm^{-1}$ respectively while that of others were below 10,000 $M^{-1}cm^{-1}$ (Table 2.1). The extraordinary high absorbance of Cu(TPA) and Cu(DMA) would be a superposition of MLCT and an additional charge transfer (CT) transition band caused by the ligands because even the absorption spectrum of TPAphen showed CT absorption band. The ligand had intrinsic CT character due to the electron donating moiety in the molecule but there was no visible light absorption (Figure 2.3). It was thought that the additional transition was ILCT(intraligand charge transition) from

electron donor moiety to phenanthorline. Therefore, Cu(TPA) and Cu(DMA) had two kinds of CT character: MLCT(from copper to phenanthorline transition) like general heteroleptic copper (I) complex and ILCT (from electron donor to phenanthorline). The ILCT transition was supported by DFT calculation below.

On the other hand, the benzonitrile moiety is strong electron withdrawing group. The extinction coefficient of MLCT transition of Cu(BZN) increased slightly to 5,700 $M^{-1}cm^{-1}$ from 5,200 $M^{-1}cm^{-1}$ of Cu(BCP). The small increase meant that electron withdrawing moiety did not make a big impact on absorption while amine based electron donating moiety of metal complexes made them to absorb visible light efficiently using CT transition.

The extinction coefficient of complexes increased slightly in order of bulkiness of the ligands: Cu(TPS), Cu(BCP) and Cu(dmphen). The TPS moiety did not affect the electronic properties much because silicon does not donate or withdraw the electron density strongly. In spite of the small electronic characteristic of the TPS, plenty of π electrons would affect the transition. As the ligand size became bulky, the extinction coefficient increased because the π electrons surrounding the bulky group contributed additional transition. It was also supported by DFT calculation below.

The λ_{max} of MLCT transition of Cu(dmphen) was 381 nm with extinction coefficient of 2,900 $M^{-1}cm^{-1}$. In order of Cu(dmphen), Cu(BCP) and Cu(TPS), the λ_{max} of MLCT were shifted to longer wavelength and the extinction coefficients also rised. The phenyl moiety in the phenanthroline ligand of Cu(BCP) and Cu(TPS) caused the bathochromic shift due to extension of the conjugation length. It lowered the LUMO energy of the complexes so MLCT

was facilitated.[17] However, the 2 nm red-shift between λ_{max} of Cu(BCP) and Cu(TPS) was not large compared with 10nm between that of Cu(dmphen) and Cu(BCP) because of the low electronic effect of TPS moiety.

Each λ_{max} of Cu(TPA) and Cu(DMA) were red-shifted to 397 nm and 401 nm respectively from 391 nm of Cu(BCP) because electron donating moieties rised HOMO energy of the complexes much. The λ_{max} of MLCT of Cu(BZN) was also red-shifted to 399 nm from 391 nm of Cu(BCP) because the BZN moiety withdrawed the electron density and lowered the LUMO energy.

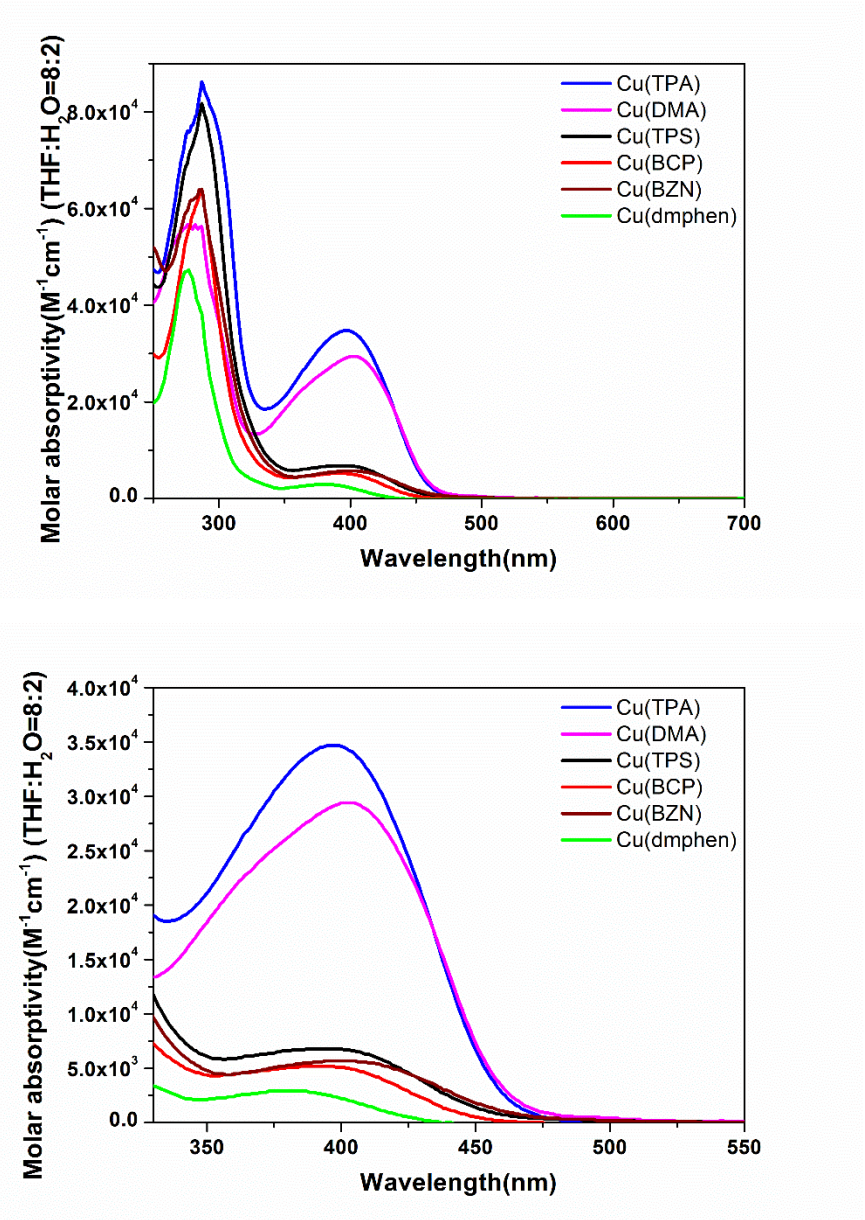

Figure 2.2. Absorption spectra of copper (I) complexes in an argon-purged mixed solution of THF:H_2O 8:2 v/v. The below figure enlarged the visible light region.

CuPS	λmax (nm)	ε ($M^{-1}cm^{-1}$)
Cu(TPA)	397	34,700
Cu(DMA)	403	29,400
Cu(TPS)	393	6,800
Cu(BCP)	391	5,200
Cu(BZN)	399	5,700
Cu(dmphen)	381	2,900

Table 2.1. Absorption properties of copper (I) complexes in an argon-purged THF:H_2O 8:2 v/v at long-wavelength region

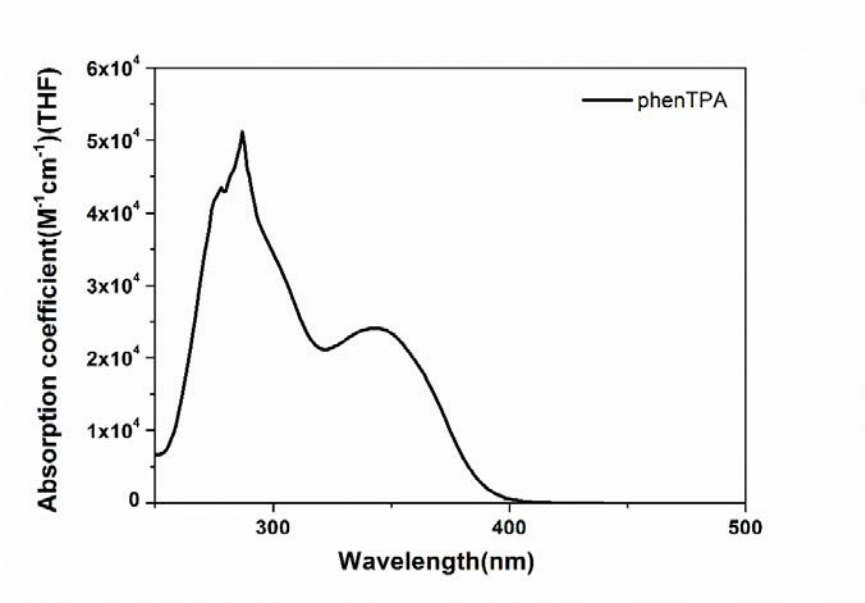

Figure 2.3. Absorption spectrum of phenTPA in an argon-purged THF solution.

We investigated the photoluminescence (PL) properties because they are essential requirements for the photosensitizer. Figure 2.4 showed the PL spectra of copper (I) complexes in each THF solution and mixed solution of THF:H_2O 8:2 v/v. The comparison was intended for an investigation into an influence of addition of water. Water is an essential proton source in the hydrogen evolution system as well as very strong lewis base. The maximum PL intensities of Cu(TPS), Cu(BCP), Cu(BZN) and Cu(dmphen) were quenched almost over 80% in the THF and H_2O mixed solution. However the intensities of Cu(TPA) and Cu(DMA) decreased just about 30%. It meant that electron donating moieties could affect the excited state dynamics of complexes and endure the quenching by water through ILCT transition.

Moreover, there are other factors to determine the photocatalytic hydrogen evolution efficiency: the excited state lifetime and non-radiatve rate constant. The electron transfer between components occurs by effective collision. If excited state of photosensitizer is quenched before the collision, the electrons cannot be transferred. Therefore photosensitizers must have sufficiently long excited state lifetime in microsecond timescale. That's why photosensitizers are usually phosphors that can utilize triplet state and have long excited state lifetime. Though all complexes in this thesis had enough lifetime for photosensitizers, generally the longer lifetime is, the more efficiently the hydrogen is produced.[13] Figure 2.5 showed that Cu(TPA) and Cu(DMA) had very long lifetime, 88.81 μs and 115.23 μs while other complexes have relatively short lifetime in 1 μs scale. Cu(BZN) have the shortest lifetime among the complexes (Table 2.2).

Not only the excited state lifetime, but also non-radiative rate constant also variable to estimate good photosensitizers. If the constant is high, the abilities of photosensitizers are wasted by thermal and vibrational energy. Table 2.2 also showed that the non-radiative rate constant of Cu(TPA) and Cu(DMA) were the smallest, $1.019 \times 10^4\ s^{-1}$ and $0.814 \times 10^4\ s^{-1}$, respectively. If there are many functional groups or branches in a molecules, it is obvious that the vibrational loss will be large. However, the non-radiative rate constant of Cu(TPA) was very low even though TPA moiety is bulky..

Cu(TPA) and Cu(DMA) exhibited the long excied state lifetime, high PLQY and low non-radiaitve decay. That would result the complexes were efficient in photocatalytic hydrogen evolution.

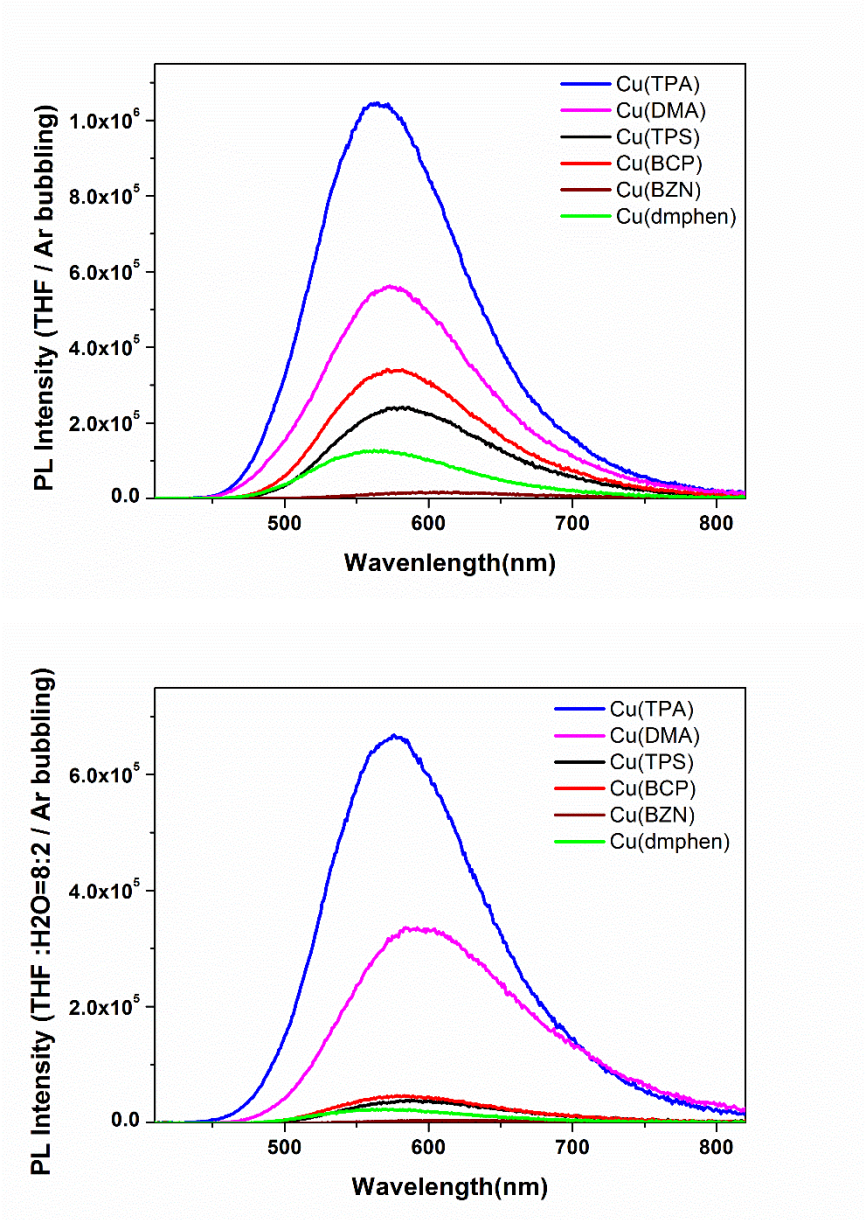

Figure 2.4. Comparison photolumienscence intensity in Ar purged THF (up) and THF:H_2O 8:2 v/v (down). Excitation at 380 nm.

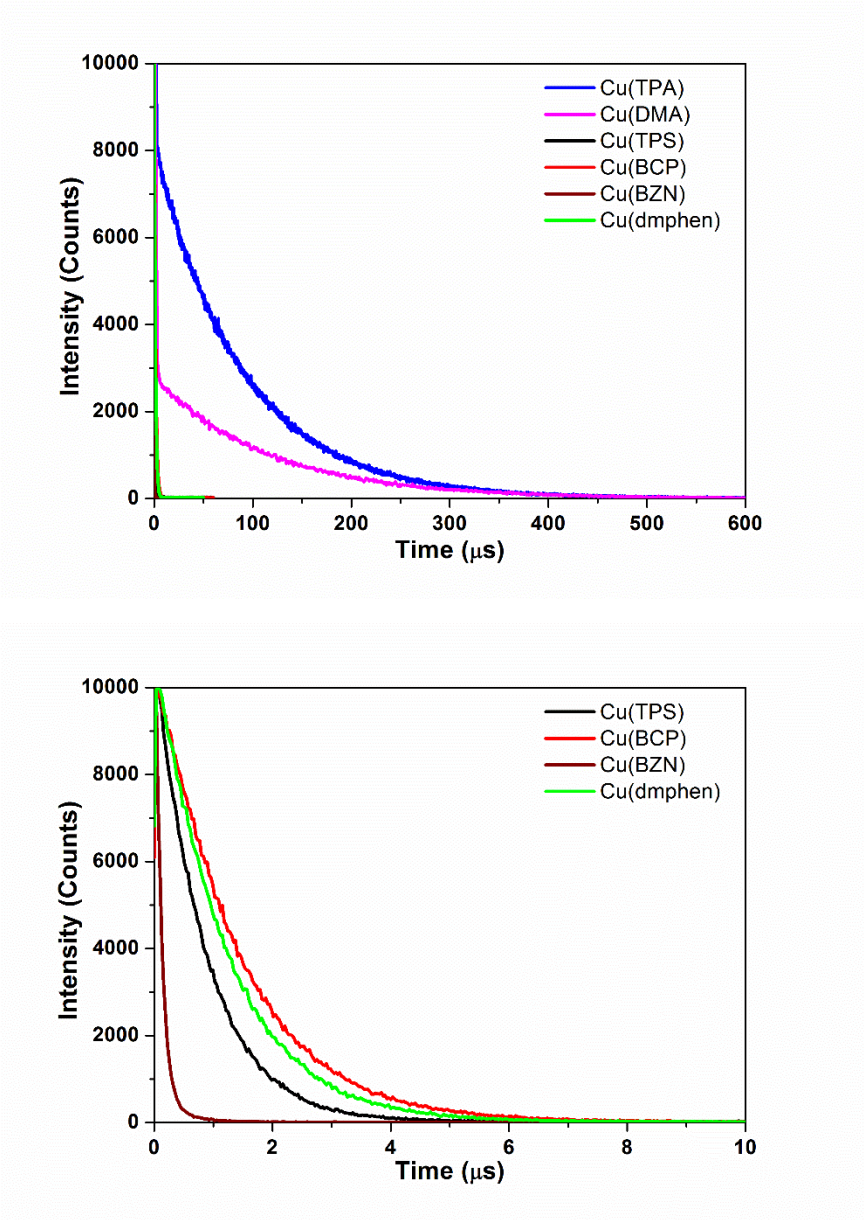

Figure 2.5. Photolumienscence decay of copper (I) complexes in an argon-purged mixed solution of THF:H_2O 8:2 v/v

CuPS	τ (μs)	PLQY (%)	k_r (10^4 s^{-1})	k_{nr} (10^4 s^{-1})
Cu(TPA)	17.29	17.65	1.021	4.763
Cu(TPS)	3.06	13.23	4.324	28.356
Cu(DMA)	287.02	8.87	0.309	0.318
Cu(BCP)	5.06	18.84	3.723	16.040
Cu(BZN)	0.36	1.12	3.111	27.467
Cu(dmphen)	4.17	14.09	3.379	20.602

CuPS	τ (μs)	PLQY (%)	k_r (10^4 s^{-1})	k_{nr} (10^4 s^{-1})
Cu(TPA)	88.31	9.99	0.131	1.019
Cu(TPS)	0.82	2.06	2.512	119.439
Cu(DMA)	115.23	6.19	0.054	0.814
Cu(BCP)	1.33	3.13	2.361	72.827
Cu(BZN)	0.22	0.20	0.909	453.636
Cu(dmphen)	1.13	2.59	2.292	86.204

Table 2.2. Excited state lifetime, PLQY, radiative rate constant and non-radiatve rate constant of copper (I) complexes in each solution (up : THF; down : THF:H_2O 8:2 v/v)

The extremely large absorption properties of Cu(TPA) and Cu(DMA) were supported by DFT calculation. Figure 2.6 and 2.7 showed the optimized geometry and frontier orbitals of copper (I) complexes. In case of a general heteroleptic complexes, HOMO is mainly localized on d-obital of copper center and diphosphine ligand. LUMO of them are localized on π electrons of phenanthroline ligand. Frontier orbitals of Cu(dmphen), Cu(BCP), Cu(BZN) and Cu(TPS) followed the tendencies (Figure 2.6). The transitions between frontier orbitals of them were MLCT according to UV/Vis by DFT calculation (Figure 2.7).

However, electron distribution of Cu(TPA) and Cu(DMA) were different from them. HOMO was localized on electron donating moiety, TPA and DMA respectively, while LUMO was localized on phenanthroline ligand (Figure 2.7). Therefore, the transitions between frontier orbitals of Cu(TPA) and Cu(DMA) were ILCT. Oscillator strengths of ILCT were higher than that of MLCT of other complexes (Table 2.4). The MLCT transitions of Cu(TPA) and Cu(DMA) were also present but they were found in higher energy side than ILCT (Figure 2.8). The MO energy diagram of each complexes showed that both of them have high energy HOMO and HOMO-1 which are located on TPA and DMA respectively (Figure 2.9). However, the orbitals below HOMO-2 were copper d-orbitals and the energy was similar to HOMO energy of other complexes. Transitions from HOMO-2, HOMO-3 and HOMO-4 to LUMO were MLCT transitions and the energies corresponded visible light. Therefore, it was demonstrated that visible light absorption band by Cu(TPA) and Cu(DMA) were superposition band of ILCT and MLCT.

As the measured UV/Vis absorption spectra of Cu(dmphen), Cu(BCP) and Cu(TPS), the UV/Vis spectra by DFT were calculated in the same way. Compared with Cu(dmphen), a phenyl ring of Cu(BCP) extended conjugation length so the MLCT absorbance increased. However, the absorbance of Cu(TPS) still increased even though TPS moiety could not affect the conjugation. It was because the large number of π electrons in TPS have portion of the transitions. The second and third transition of Cu(TPS) calculated by DFT were from copper d-orbital and π electrons in TPS to phenanthroline orbitals. Cu(dmphen) and Cu(BCP) does not have the ILCT transitions like Cu(TPS). Therefore, the ligand size also can affect visible light absorbance.

The unprecendented PL properties of complexes with electron donating moiety were also supported by DFT calculation. Before we describe that, the structure of copper (I) complexes should be understood. The ground structure of copper (I) complexes is tetrahedral. If it is excited, MLCT transition occurs. Electrons in copper center moves to ligands then copper (I) is oxidized to copper (II). Because copper (II) favours the square planar sturcutre, the copper complex structure is distorted. After distortion, the complex can be attacked easily by Lewis bases such as solvent or counter ions toward its z-axis of d-orbital then exciplex quenching occurs. This is the intrinsic problem of copper (I) complexes which have low PLQY in solutions.

In contrast, the HOMO of Cu(TPA) and Cu(DMA) located in electron donating moieties. Therefore, the frontier orbital transition of the complexes was ILCT, not MLCT. The excited state of the complexes by ILCT transition maintained the oxidation state to Cu (I). The structure was not distorted then

the exciplex quenching did not occur. Consequently, the extraordinary photophysical properties of complexes with electron donating moieties were achieved through another excitation, ILCT.

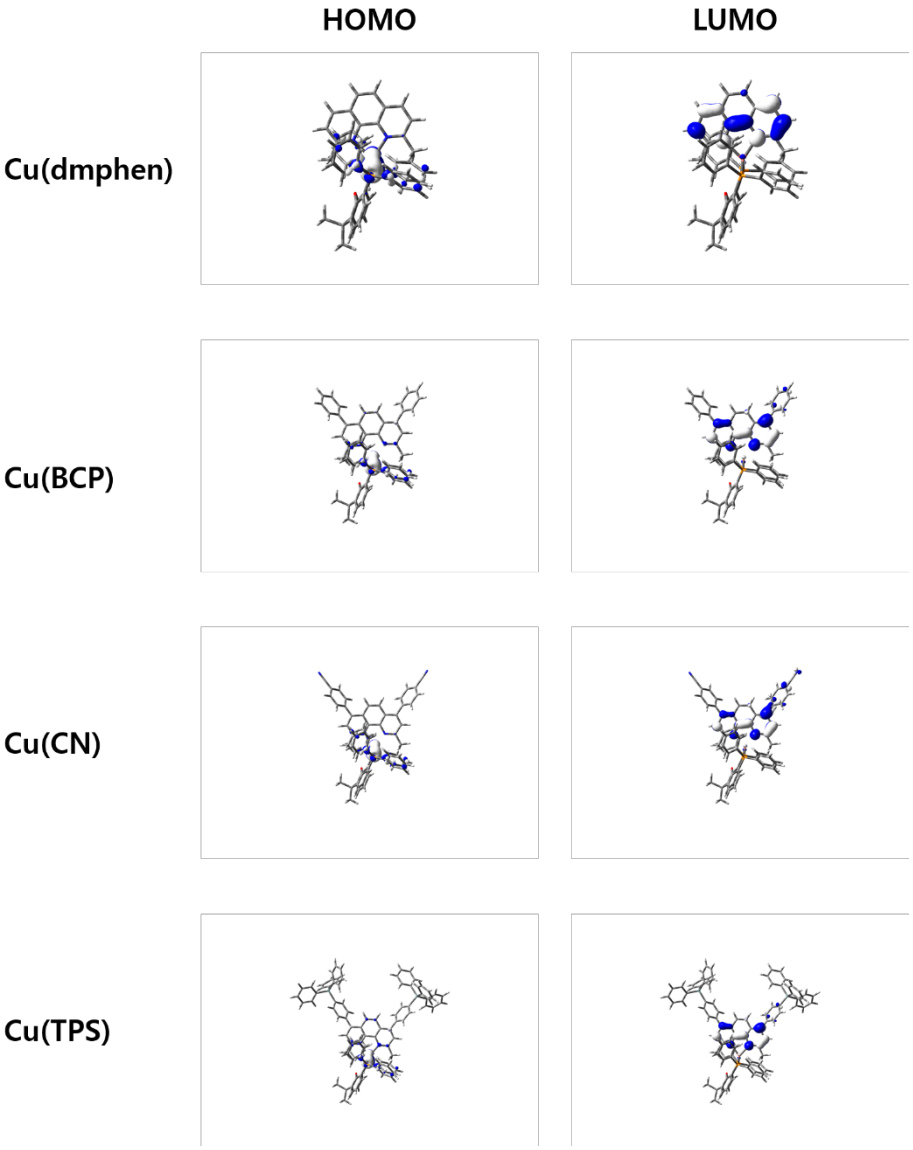

Figure 2.6. Frontier orbitals of Cu(dmphen), Cu(BCP), Cu(BZN) and Cu(TPS)

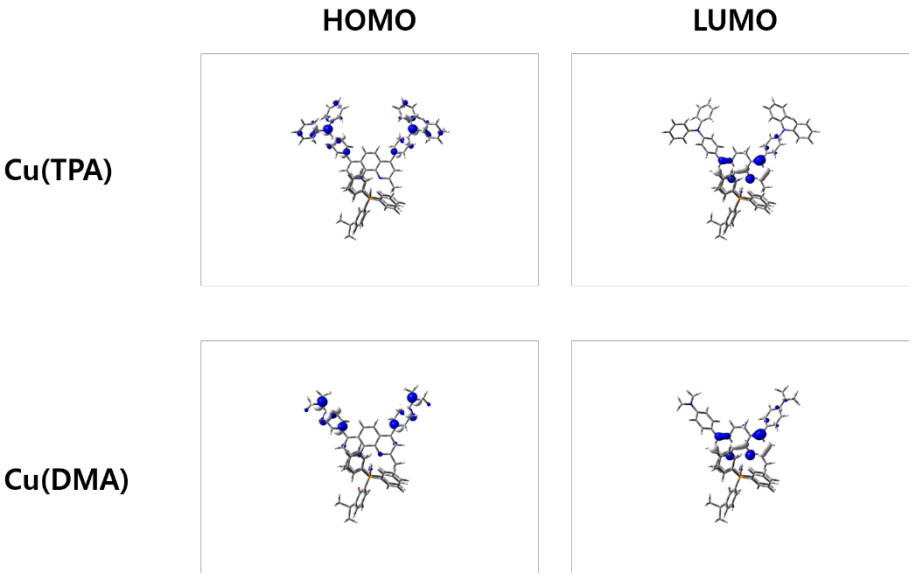

Figure 2.7. Frontier orbitals of Cu(TPA), Cu(DMA)

CuPS	Oscillator strength	Character
Cu(TPS)	0.1341 (388.70 nm)	Copper → phen
	0.0017 (379.93 nm)	Copper+TPS → phen
	0.0053 (364.15 nm)	Copper+TPS → phen
Cu(BCP)	0.0929 (391.47 nm)	
	0.0012 (382.06 nm)	Copper → phen
	0.0050 (367.43 nm)	
Cu(BZN)	0.0907 (415.38 nm)	
	0.0007 (397.30 nm)	Copper → phen
	0.0346 (392.78 nm)	
Cu(dmphen)	0.0419 (394.55 nm)	
	0.0004 (380.90 nm)	Copper → phen
	0.0051 (375.04 nm)	
Cu(TPA)	0.3444 (486.89 nm)	TPA → phen
	0.1295 (484.01 nm)	TPA → phen
	0.1862 (463.30 nm)	TPA → phen
	0.2028 (451.92 nm)	TPA → phen
	0.0539 (377.43 nm)	Copper → phen
	0.0100 (375.62 nm)	Copper → phen
Cu(DMA)	0.2156 (436.37 nm)	DMA → phen
	0.1924 (429.09 nm)	DMA → phen
	0.1828 (417.11 nm)	DMA → phen
	0.2165 (403.47 nm)	DMA → phen
	0.0207 (367.28 nm)	Copper → phen
	0.0057 (351.88 nm)	Copper → phen

Table 2.3. Calculated oscillator strength of major transitions of CuPSs. Phen representatives phenanthroline

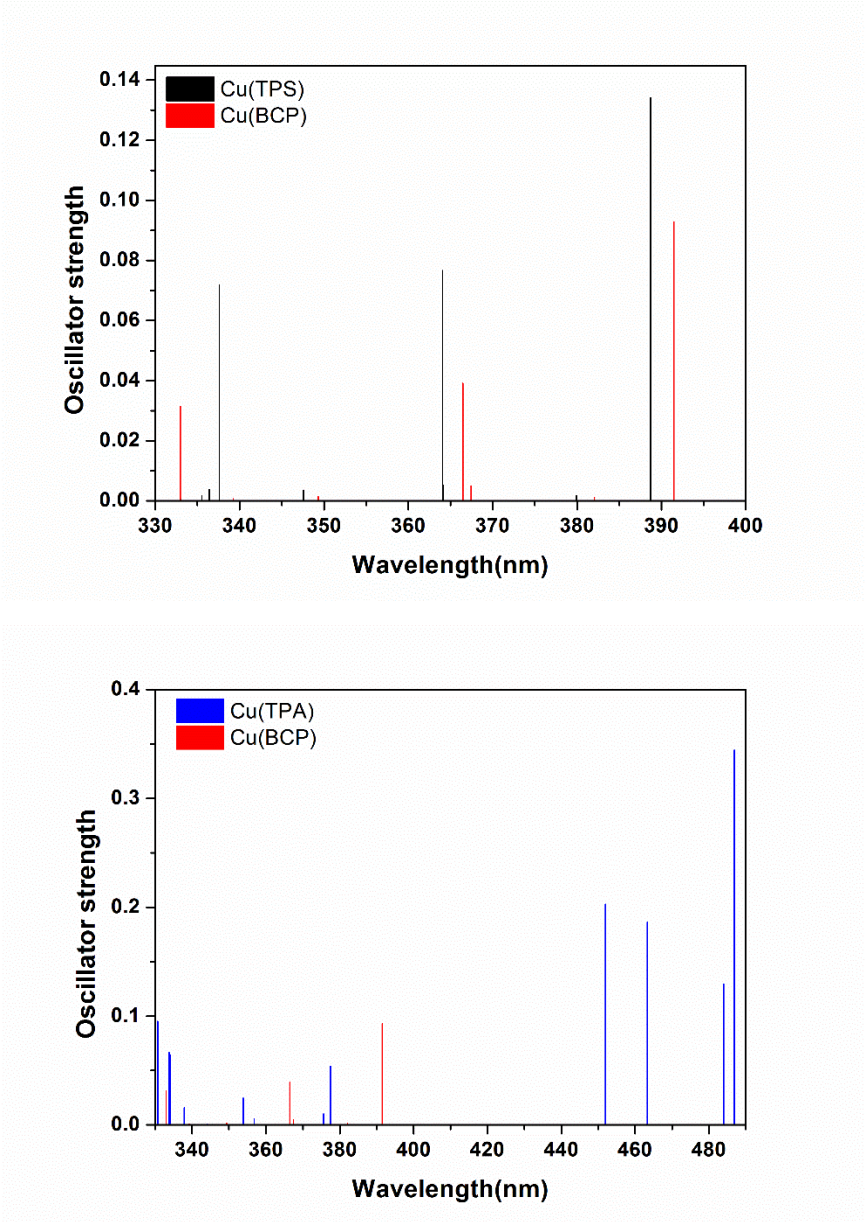

Figure 2.8. Oscillator strength comparison at long wavelength region (up : Cu(TPS) and Cu(BCP); down : Cu(TPA) and Cu(BCP))

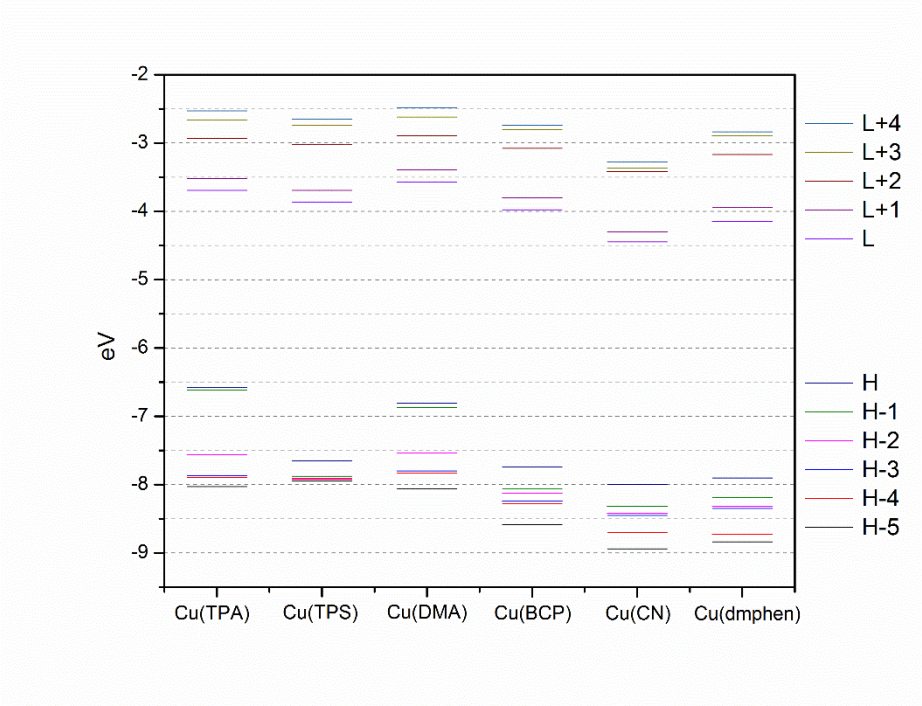

Figure 2.9. Calculated MO energy diagram of CuPSs

In our previous studies, iridium (III) photosensitizers with bulky moieties exhibited enhanced durability and led to high TONs. Wu group reported about copper (I) photosensitizer that only a phenyl group at periphery of phenanthroline ligand could protect the excited state then resulted the high efficiency of hydrogen evolution.[22] To examine whether bulky moieties such as TPA and TPS would also act protecting groups of copper (I) complexes, photodegradation experiments were carried out in an argon-purged mixed solution (10 μM) of THF:H_2O 8:2 v/v and irradiated with visible light for 4 hours. The absorption spectra were recorded every hour (Figure 2.10). The extinction coefficients of the MLCT band were measured with time because it stands for the coordination between ligands and metal center.

The decrease of MLCT of Cu(TPA) and Cu(TPS) were 3.96% and 4.54% and the values were the lowest (Table 2.5). Therefore, the bulky moieties of the complexes could protect the complexes and enhanced photostability.

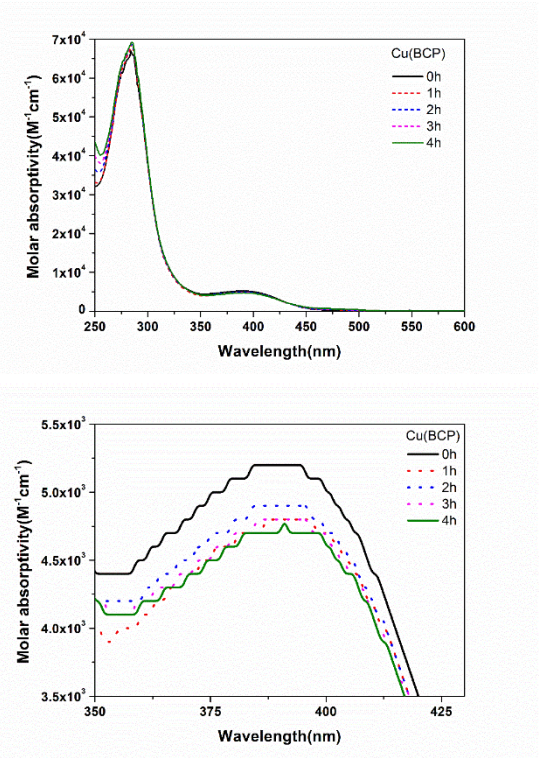

Figure 2.10. Absorption spectral change of CuPSs during photoirradiation. Each solutions contains 10μM copper (I) complexes in THF:H_2O 8:2 v/v. The solution were irradiated by Xe lamp with 400 nm cut-off filter.

CuPS	Decreased extinction coefficient
Cu(TPA)	3.96 %
Cu(DMA)	10.88 %
Cu(TPS)	4.54 %
Cu(BCP)	7.69 %
Cu(BZN)	6.78 %
Cu(dmphen)	9.09 %

Table 2.4. The decreased extinction coefficient during 4 hours of irradiation.

When a heteroleptic copper (I) complex dissolved in solution, the ligands can be dissociated and redistributed to homoleptic complexes which is expressed $Cu(NN)_2$.[14] During the photocatlytic hydrogen evolution, it happens too. However, the homoleptic complexes such as $Cu(TPS)_2$ or $Cu(BCP)_2$ could not act as photosensitizers because there were little hydrogen evolved during the hydrogen evolution experiment with the homoleptic complexes instead of heteroleptic complexes. Therefore, if the amount of homoleptic complex increase much more, that of active heteroleptic complex decrease then the hydrogen evolution efficiency are also lowered..

ESI-MS data collected from reaction mixture before and after irradiation for 24 hours revealed that homoleptic complex ($[M\text{-}PF_6^-]$ = 784.26) was formed when the photosensitizer was Cu(BCP) (Figure 2.11). However, when the photosensitizer was Cu(TPS) which have bulky moiety in the ligand, there was no homoleptic complex ($[M\text{-}PF_6^-]$ = 1816.6) at all (Figure 2.12). The results supported the role of bulky moiey of complexes for high stability.

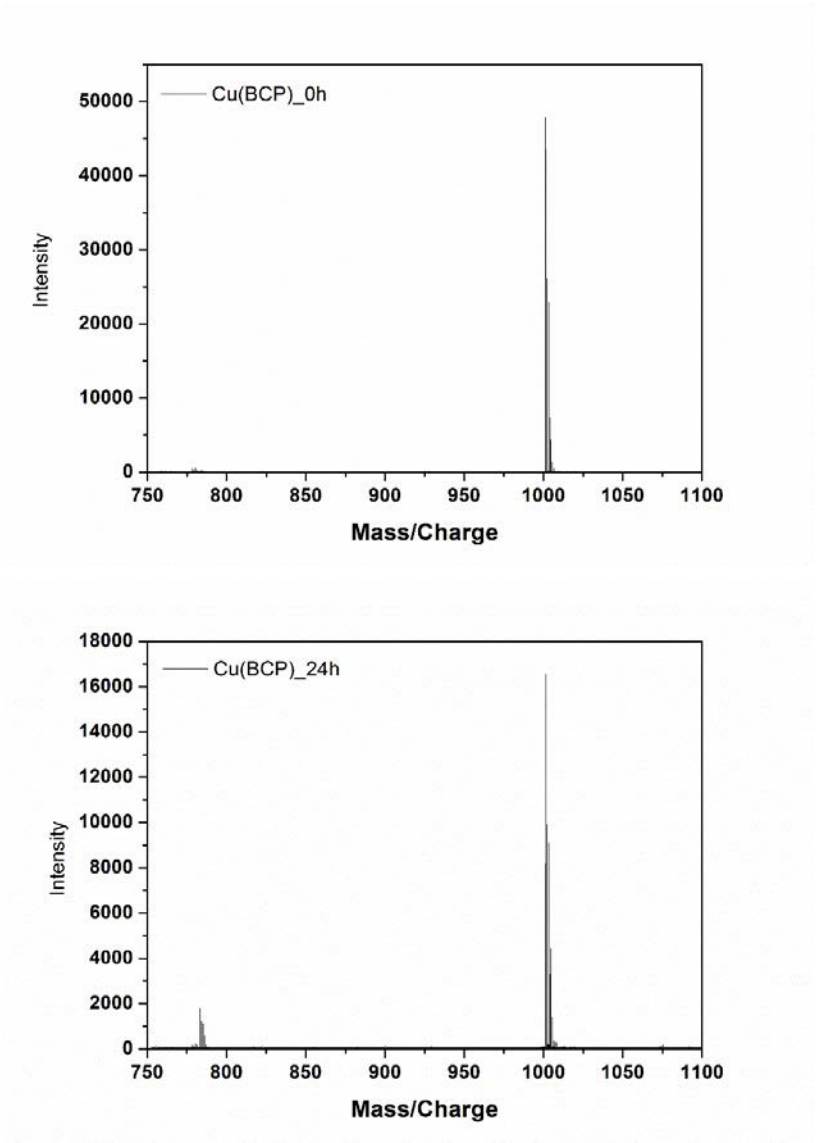

Figure 2.11. ESI mass of Cu(BCP) before and after the photocatalytic hydrogen evolution with colloidal Pt in mixed solution of THF:H_2O:TEA for 24 hours. ([M-PF_6^-] = 784.26)

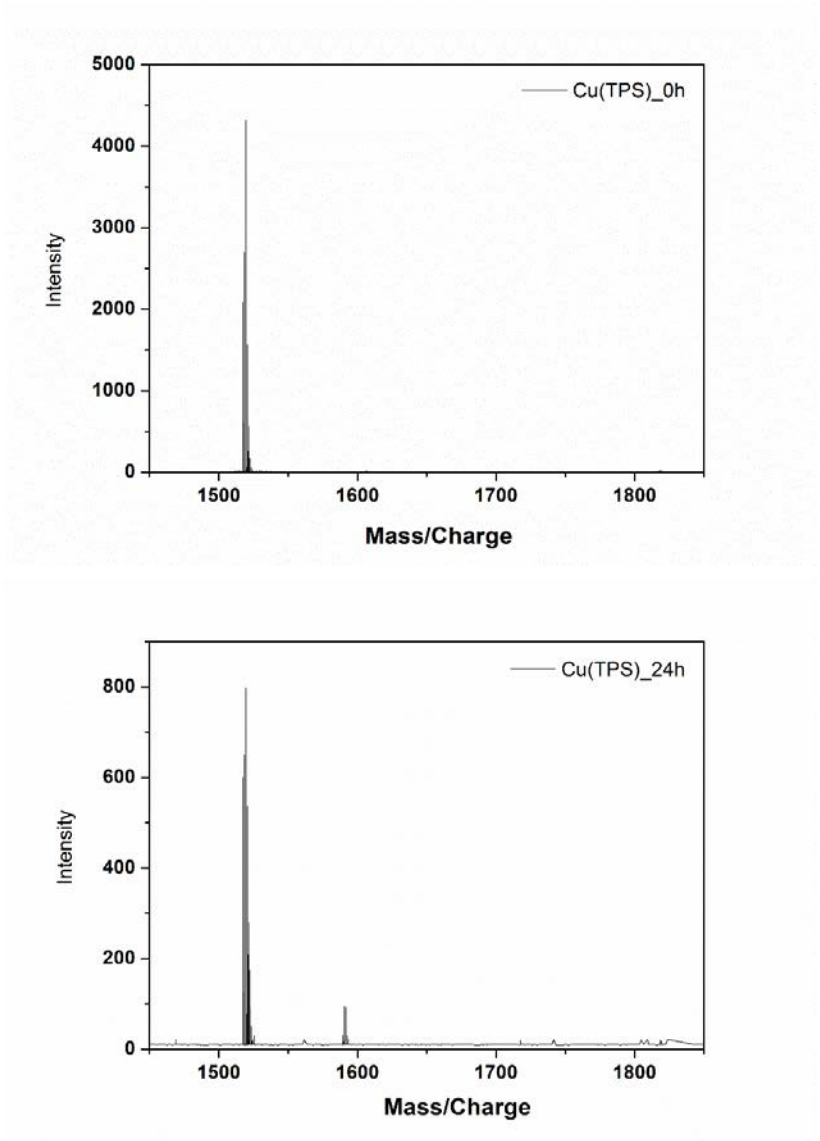

Figure 2.12. ESI mass of Cu(TPS) before and after the photocatalytic hydrogen evolution with colloidal Pt in mixed solution of THF:H_2O:TEA for 24 hours. ([M-PF_6^-] = 1816.6)

To ascertain the photocatalytic efficiency depending on the photophysical properties and stability of copper (I) complexes, hydrogen evolution experiments were carried out in a mixture of THF and H_2O with TEA as sacrificial reagent. 0.5 μmol of photosensitizers except Cu(TPA) and 0.5 μmol of WRC were dissolved in the 8 mL of THF, 2 mL of H_2O and 2 mL of TEA. In case of Cu(TPA), because hydrogen evoloved too much and GC could not detect, all amounts and volumes were reduced half : 0.25 μmol of Cu(TPA) and WRC in 4 mL of THF, 1 mL of H_2O and 1 mL of TEA. The samples were irradiated by visible light excluding ultraviolet light by 400 nm cutoff filter. K_2PtCl_4 is reduced with hydrogen then becomes a colloidal Pt as a actual water reduction catalysis in the solution while the photocatalysis.[19,20]

Under the above condition, the TON of 18299 was recorded when Cu(TPA) was used as CuPS for 96 hours (16069 for 47 hours) (Figure 2.13, 2.14). The TON was very outstanding value compared with that of other photosensitizers used in this research. Cu(BCP), which was reported in previous paper,[13] showed only TON of 2038. The TON of Cu(TPA) was about 10 times to that of Cu(BCP). It was the highest value among the copper (I) photosensitizers reported so far and even higher than TONs of noble metal complexes such as iridium (III) or ruthenium (II) complexes. It meant that it could endure the catalytic cycle containing photoexcitation, reduction and returning back to ground state without decomposition in many times. Not only TON, but also TOF of Cu(TPA) was very high, 1817.6 h^{-1}. The TOF of Cu(TPA) is also about more than 10 times to that of Cu(BCP), 131.8 h^{-1}.

The 2nd efficient photosensitizer was Cu(TPS) with bulky triphenylsilyl

moiety. It recorded TON of 6,521 for 48 hours. The TOF of 332.8 h^{-1} was also the high value compared to other photosensitizers. The following efficient photosensitizer was Cu(DMA). The TON of Cu(DMA) was 3,184 for 48 hours and it was higher than 2,038 of Cu(BCP). The Cu(DMA) have the ligands which contains electron donating moiety like Cu(TPA). However, Cu(BZN) which have electron withdrawing moiety showed the worst TON of 586 among the photosensitizers except the unfunctionalized Cu(dmphen). The results meant that electron donating moieties could improve the photocatalytic acitivity of photosensitizers.

Even though photosensitizers which have large and electron donating moieties showed high TON, the rate of photocatalysis did not follow the tendency. Cu(DMA) showed the high TON of 3,184 but the TOF of 129.1 h^{-1} was very poor. The TOF was not different much with Cu(BCP) which had TOF of 131.8. In case of Cu(BZN), the TON of 586 was very poor but TOF of 162.7 h^{-1} was moderate. The catalyst, sacrificial reagent and solvent conditions were same in the experiments. Therefore the rate determining steps of hydrogen evolution should be photocatalysis process of photosensitizers including absorbing visible light and electron transfer from sacrificial reagent to excited state photosensitizer.

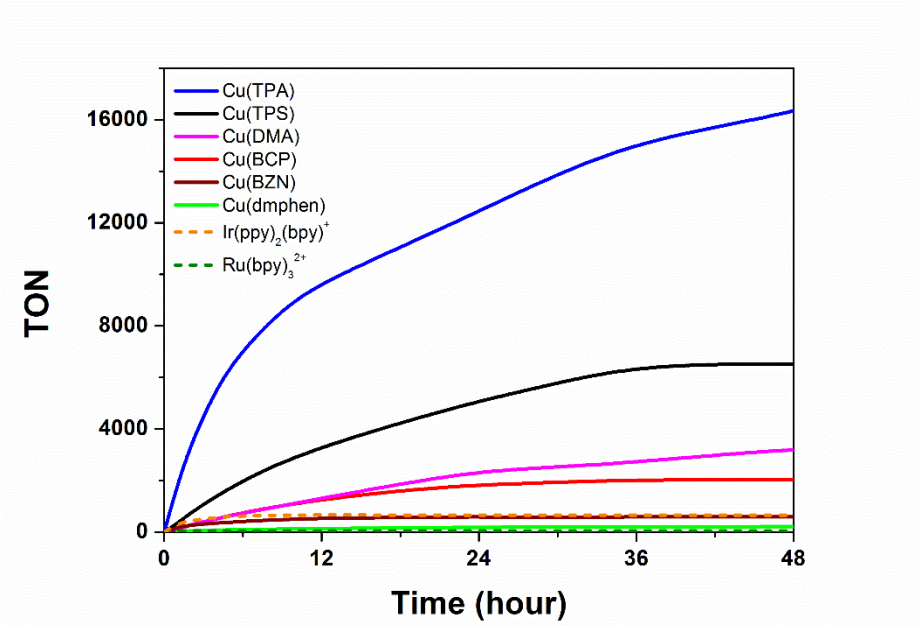

Figure 2.13. Photocatalytic hydrogen evolution curve. The solution contained 0.5 μmol CuPS, 0.5 μmol K_2PtCl_4, 2 mL of H_2O, 2 mL of TEA and 8 mL of THF in a 40 mL air-tight vial. The vial was irradiated with a 300 W Xe lamp with a 400 nm cut-off filter. TON = n(H)/n(Cu).

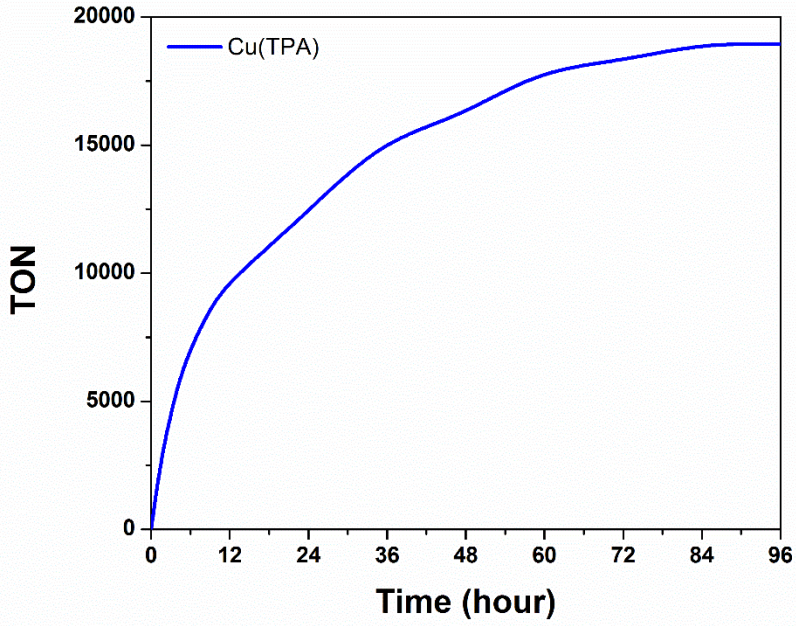

Figure 2.14. Photocatalytic hydrogen evolution curve of Cu(TPA) for 4 days until hydrogen evolution ceased. The experimental condition was same to Figure 2.13

CuPS	TON	Time (h)	TOF (h^{-1})
Cu(TPA)	18,974 (16,070)	96 (47)	1817.6
Cu(TPS)	6,521	46	332.8
Cu(DMA)	3,184	48	129.1
Cu(BCP)	2,038	46	131.8
Cu(BZN)	586	24	162.7
Cu(dmphen)	203	48	19.9
$Ru(bpy)_3^{2+}$	39	6	
$Ir(ppy)_2(bpy)^+$	649	17	

Table 2.5. Comparison of TONs and TOFs of hydrogen evolution with CuPSs and Pt colloid in THF, TEA, H_2O mixed solution

Photocatalytic hydrogen evolution is sensitive to conditions such as polarity and coordinating ability of solvent, pH, sacrificial reagent and concentration of each components. I investigated how the different solvents or sacrificial reagents affect the hydrogen evolution tendency. Figure 2.15 showed that hydrogen evolution curve with DMF as solvent and DMA as sacrificial reagent instead of THF and TEA when Cu(TPS), Cu(BCP) and Cu(dmphen) were photosenstiziers.

The TON and TOF values were changed compared with expriments with mixture of THF and H_2O (Table 2.7). TON of Cu(TPS) decreased to 3352 while that of Cu(BCP) was almost same and that of Cu(dmphen) increased to 925. However, as ever, Cu(TPS) were more efficient than Cu(BCP) following Cu(dmphen). And the lifetimes of hydrogen evolution were extended. Even though the values were different, the efficiency were similar regardless of the solvent conditions.

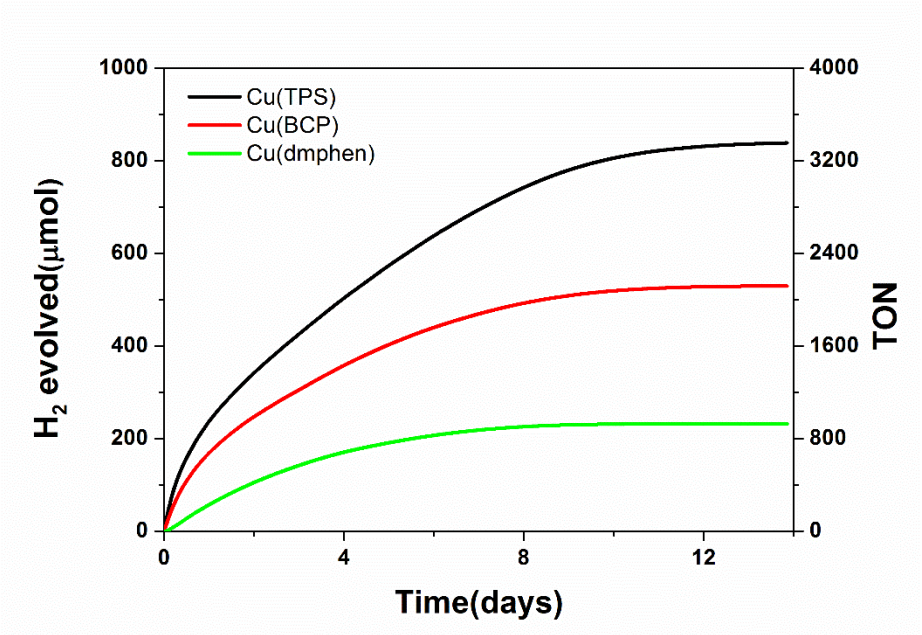

Figure 2.15. Photocatalytic hydrogen evolution curve. The solution contained 0.5 μmol CuPS, 0.5 μmol K_2PtCl_4, 2 mL of H_2O, 2 mL of DMA and 8 mL of DMF in a 20 mL air-tight vial. The vial was irradiated with a 300 W Xe lamp with a 400 nm cut-off filter. TON = n(H)/n(Cu).

CuPS	TON
Cu(TPS)	3,352
Cu(BCP)	2,117
Cu(dmphen)	925

Table 2.6. Comparison of TONs and TOFs of hydrogen evolution with CuPSs and Pt colloid in DMF, DMA, H_2O mixed solution

To attain total noble-metal-free system, previeous researches done by Beller group reported that they have used triiron catalyst, $Fe_3(CO)_{12}$, as WRC with photosensitizers.[12,13,17,22-24] However, stability of triiron catalyst is so low that it is decomposed during the catalysis and black precipitate is formed by agglomeration of iron atoms.[24] On investigation of the hydrogen evolution curve, the faster hydrogen was evolved, the sooner the production ceased (Figure 2.17). It is deducible that the triiron catalyst degradation is fast when the photocalalysis is rapid. In addition, triiron catalyst, $Fe_3(CO)_{12}$, becomes to more active iron catlalyst, $[Fe_2(CO)_7PPh_2]^-$, during the hydrogen evolution.[24] The phosphine comes from the heteroleptic copper (I) complex with diphosphine. Because of the active catalyst, the hydrogen evolution rate after several hours is faster than initial rate. However, it facilitates the degradation of photosensitizers.

During hydrogen evolution experiment with 0.5 μmol of each photosensitizer and 1 μmol of triiron catalyst, TOF of Cu(TPA) was the highest following Cu(TPS) and Cu(BCP). But the hydrogen evolution with Cu(TPA) ceased the earliest and resulted low TON (Figure 2.16). I did the same experiment for a same time but added triiron catalyst twice as much as before: 2 μmol. The lifetime of hydrogen evolution increased twice because the amount of catalyst doubled. The TON of Cu(TPA) increased and showed the hightest among the photosensitizers according to extended lifetime however that of Cu(BCP) decreased inspite of extended lifetime. However, TOF of all photosensitizers decreased because when the amount of catalyst was much than of photosensitizer, two electron transfer to one catalyst was harder. And catalyst

itself can absorb visible light and block the photosensitizers.

Another researches reported by Castellano et al. used the cobalt catalyst, $Co(dmgH)_2(py)(Cl)$.[12] I applied the catalyst to hydrogen evolution experiments with the photosensitizers. Cu(TPA) and Cu(TPS) showed high TOF and Cu(BZN) showed low TOF like the experiments explained above (Figure 2.18). However, all of TONs of photosensitizers were similar, about 160. Because the cobalt catalyst was not stable, it was the boundary condition. The hydrogen was evolved until all cobalt catalyst molecules were decomposed rapidly.

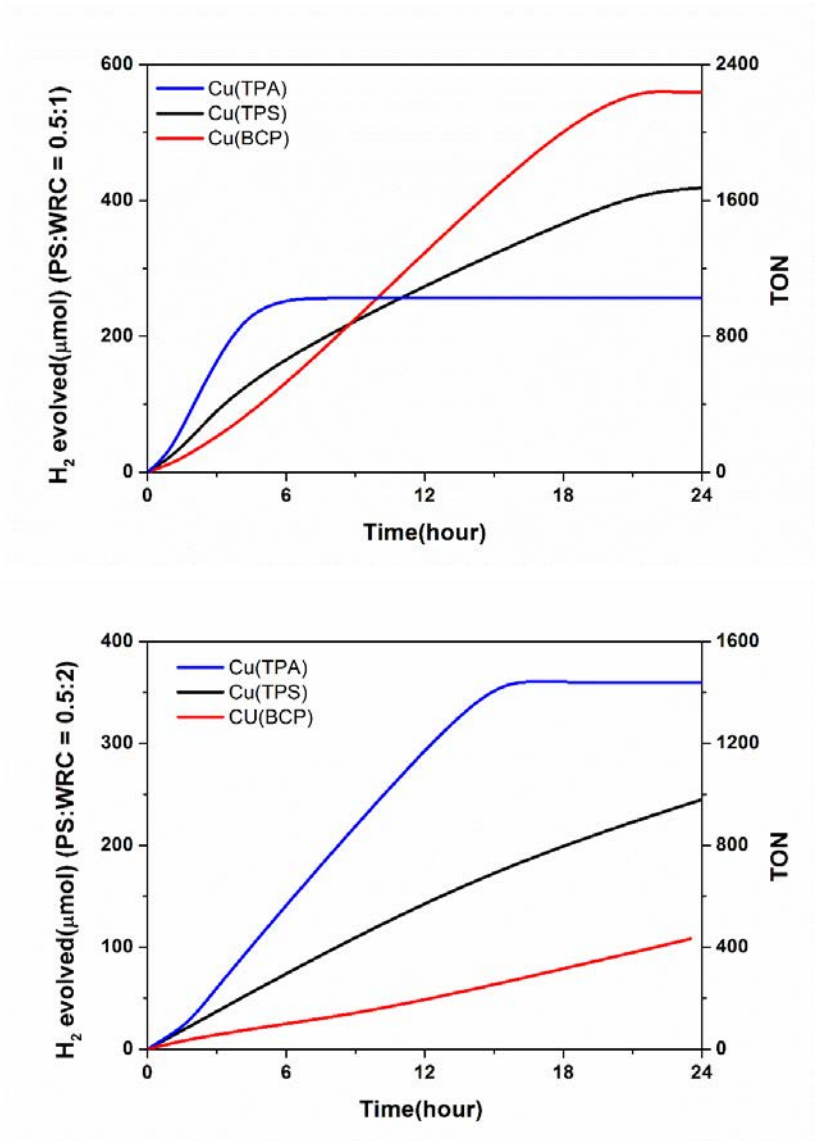

Figure 2.16. Photocatalytic hydrogen evolution curve. The solution contained 0.5 μmol CuPS, $Fe_3(CO)_{12}$(up : 1 μmol; down : 2 μmol), 2 mL of H_2O, 2 mL of TEA and 8 mL of THF in a 40 mL air-tight vial. The vial was irradiated with a 300 W Xe lamp with a 400 nm cut-off filter. TON = n(H)/n(Cu).

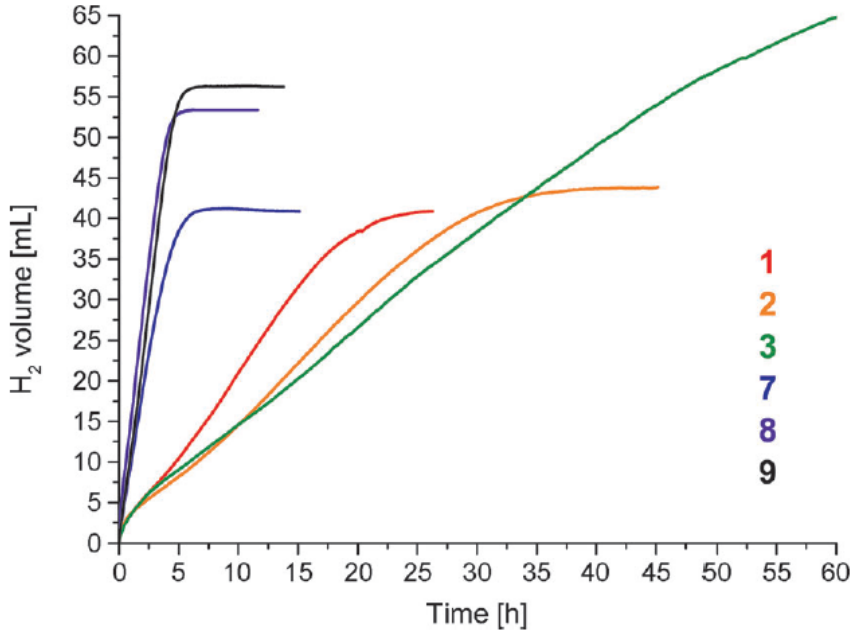

Figure 2.17. Previous reported hydrogen evolution curve using $Fe_3(CO)_{12}$[13]

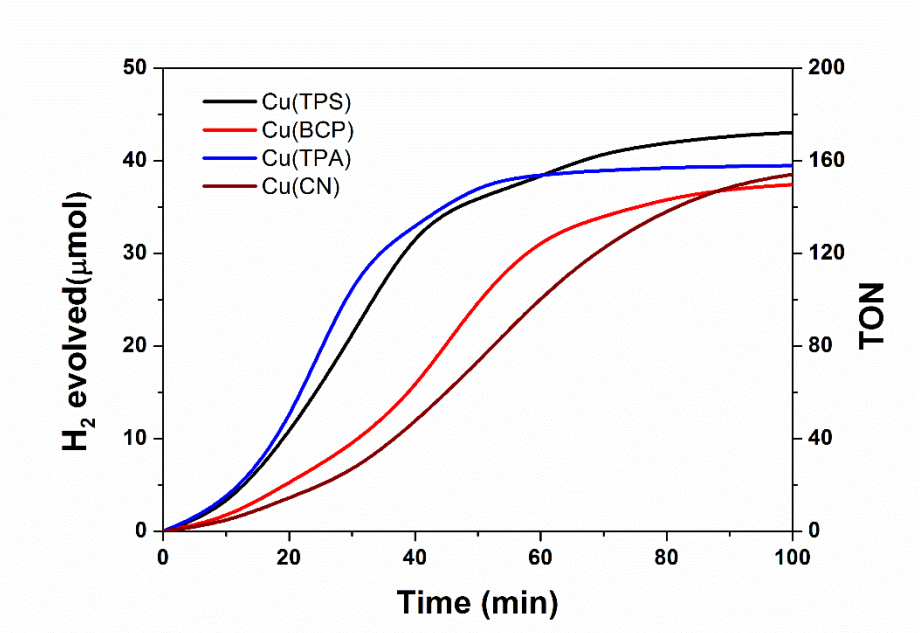

Figure 2.18. Photocatalytic hydrogen evolution curve. The solution contained 0.5 μmol CuPS, 2 μmol $Co(dmgH)_2(py)(Cl)$, 2 mL of H_2O, 2 mL of TEA and 8 mL of THF in a 40 mL air-tight vial. The vial was irradiated with a 300 W Xe lamp with a 400 nm cut-off filter. TON = n(H)/n(Cu).

According to hydrogen evolution curve, TOF varied with the ligands. it was thought that the rate determining steps depend on the photosensitizers. The more photons are absorbed by photosensitizers, the faster the hydrogen is evolved. In addition, thermodynamic factor also should be considered because light absorption is followed by reductive quenching. The driving force can be estimated based on the Rehm-Weller equation which is used in calculating free energy for photoinduced electron transfer.

$\Delta G = E(D^+/D) – E(A/A^-) - \Delta E_{00} + w_p$

ΔG is free energy and each $E(D^+/D)$, $E(A/A^-)$ are redox potential of electron donor or acceptor. ΔE_{00} is the transition energy between vibrationally relaxed ground and excited state. The last term is the Coulomb work term but I approximated to zero because of its small portion.

The quenching is redox reaction between excited state of photosensitizers and TEA as electron donor. The potential of each component should be matched for the redox reaction. I measured redox potentials of all photosensitizers and TEA using cyclic voltammetery (Figure 2.19). However, the potential measured by cyclic voltammetry is about ground state of complexes. Because the excited state of photosensitizer is reduced by TEA, the potentials must be corrected to excited state redox potentials. They can be calculated in the following formulas.[25]

$E^*_{red} = E_{red} + E_{00}$

$E^*_{ox} = E_{ox} – E_{00}$

As the calculation result, all E^*_{red} of photosensitizers were positive than E_{ox} of TEA. They can be reduced by TEA thermodynamically (Table 2.8). Here,

E^{*}_{red} is same to ($E(A/A^{-}) + \Delta E_{00}$) of Rehm-Weller equation above. Therefore, the free energy from Rehm-Weller equation is the difference between oxidation potential of TEA and excited state reduction potential of photosensitizers. From the data, it could be inferred that driving force for reductive quenching of Cu(DMA) was the weakest because free energy of Cu(DMA) is the lowest (Table 2.7).

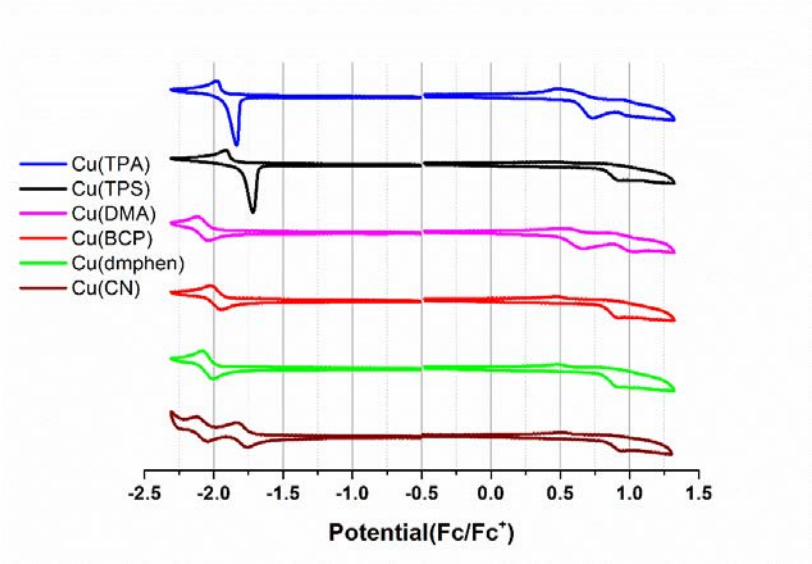

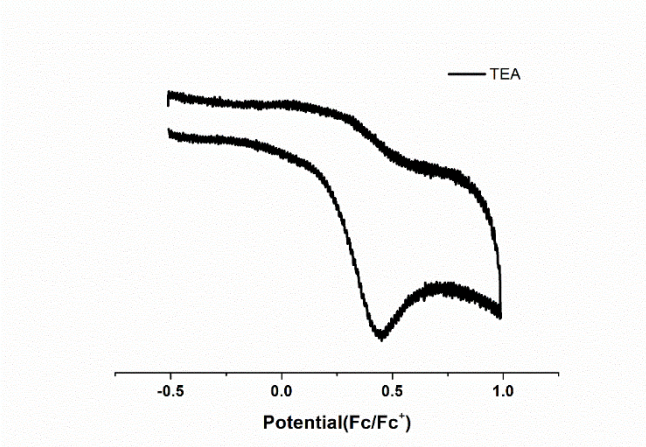

Figure 2.19. Cyclic voltammograms of photosensitizers (up) and TEA (down) in Ar-purged acetonitrile containing 0.1 M tetrabutylammonium heafluorophosphate as a supporting electrolyte with a scan rate of 100mV/s.

CuPS	E_{red} (V)	E_{ox} (V)	E_{00} (eV)	E^*_{red} (V)	ΔG (eV)
Cu(TPA)	-1.93	0.61(1^{st}) 0.93(2^{nd})	2.463	0.533	-0.323
Cu(TPS)	-1.86	0.81	2.556	0.596	-0.486
Cu(DMA)	-2.00	0.51(1^{st}) 0.91(2^{nd})	2.492	0.492	-0.282
Cu(BCP)	-1.91	0.80	2.480	0.570	-0.360
Cu(dmphen)	-1.98	0.80	2.538	0.558	-0.348
Cu(BZN)	-1.73(1^{st}) -2.03(2^{nd})	0.83	2.526	0.796	-0.586
TEA		0.21			

Table 2.7. Redox potentials of ground state and excitd state of photosensitizers and TEA. The potentials were calibrated with the Fc/Fc+ reference electrode

I investigated quenching tests by TEA to verify whether Cu(DMA) has poor ability for reductive quenching. If an excited state of photosensitizer is quenched by TEA, the photoluminescence intensity of photosensitizer will decreases. I compared Cu(TPA) and Cu(DMA) in the experiment because the two complexes had similar photophysical properties inclucing light absorption. In this test, the solvent was the mixture of THF, H_2O and TEA. As volume of TEA increased from 0 to 2 mL, that of THF decreased to fix the total volume of 12 mL. The amount of photosensitizers was 0.5 μmol such as the hydrogen evolution experiment.

When the volume of TEA increase from 0 to 2 mL, the maximum photoluminescence intensity of Cu(TPA) decreased almost by 79% (Figure 2.20). However, that of Cu(DMA) decreased by only 49%. It meant that Cu(DMA) was not quenched by TEA well compared to Cu(TPA). The result corresponded the prediction result from comparison of free energy for electron transfer. The excited state of photosensitizer is quenched by collison with TEA as a quencher. The bimolecular quenching rates of Cu(TPA) and Cu(DMA) with TEA were calculated from stern-volmer quenching rate and excited state lifetime (Figure 2.21). The biomolecular quenching rate of Cu(TPA) and Cu(DMA) was 26.0 $M^{-1}\mu s^{-1}$ and 7.1 $M^{-1}\mu s^{-1}$ respectively. Therefore, Cu(DMA) is not quenched by TEA well and it affects the hydrogen evolution rate. (Table 2.8)

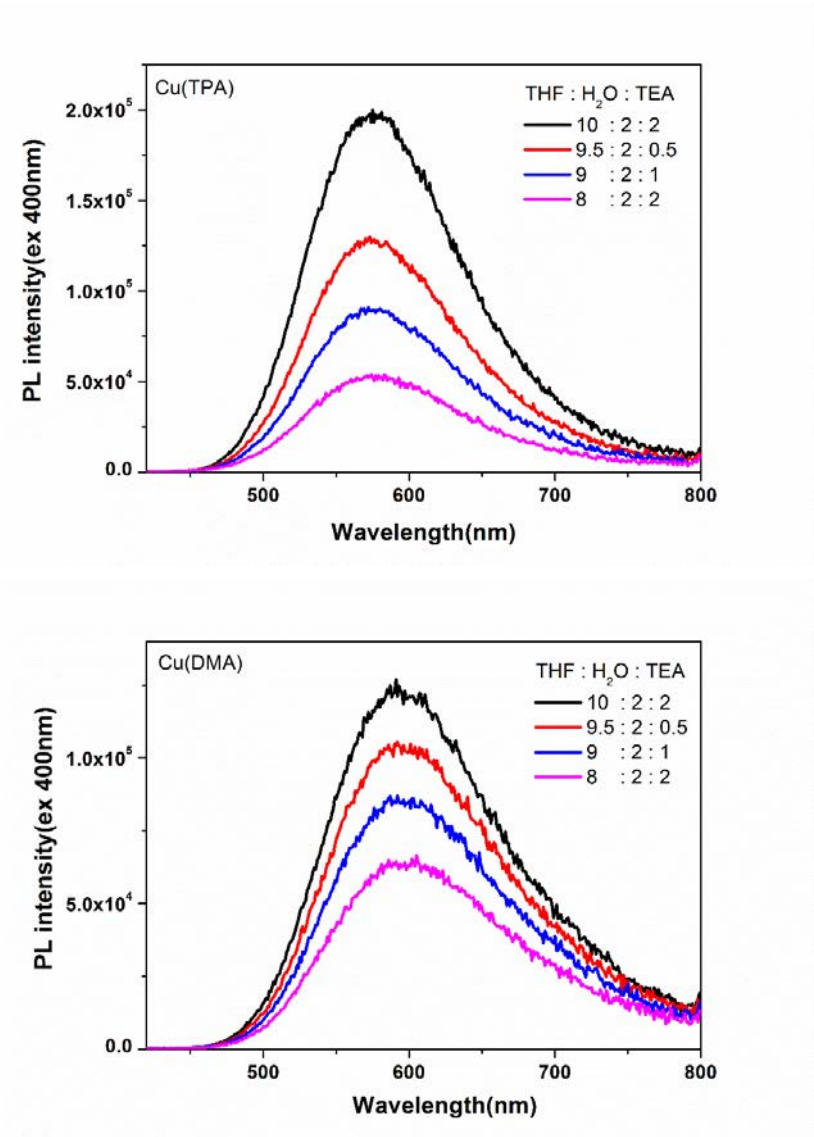

Figure 2.20. Photoluminescence quenching of Cu(TPA) (up) and Cu(DMA) (down) solution by addition of TEA in Ar-purged mixed solution of THF, H_2O and TEA. Excitation at 400nm

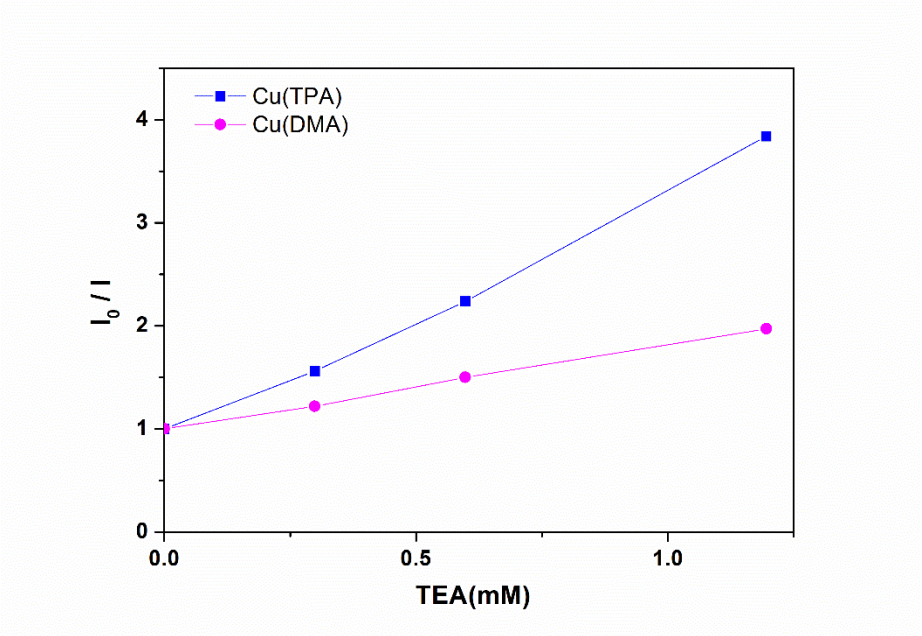

Figure 2.21. Stern-Volmer curves for the quenching of Cu(TPA) and Cu(DMA) by TEA. $I_0/I = 1 + K_{SV}[Q]$. Excitation at 400nm.

CuPS	**K_{SV} (M^{-1})**	**τ (μs)**	**K_q ($M^{-1}\mu s^{-1}$)**
Cu(TPA)	2,292.1	88.31	26.0
Cu(DMA)	812.9	115.23	7.1

Table 2.8. Stern-Volmer constant(K_{sv}) and bimolecular quenching constant(K_q). $K_q = K_{sv} / \tau$.

In consequence, the rate of hydrogen evolution is dependent on both visible light absorption and free energy for electron transfer. The more photosensitizers absorb visible light, the faster hydrogen is evolved. Moreover, the redox potential between excited state of photosensitizer and TEA should be appropriate for reductive quenching. Cu(TPA) meets the two requirements and showed significantly high TOF. On the other hand, Cu(DMA) showed low TOF in spite of its large visible absorption ability because its free energy is relatively low.

2.4 Conclusions

In summary, the copper (I) photosensitizers with different electronic characters and size of ligands were designed and synthesized. The photosensitizers with electron donating moieties exhibited long excited state lifetime, high PLQY and low non-radiative rate constant through ILCT preventing the distortion of the structure. The enhanced photoluminescence properties as well as large extinction coefficient affected the highly efficient photocatalytic hydrogen evolution with the highest TON of 18299 reported to date. In addition, the bulkiness of the ligands also increased the rate of hydrogen evolution and the photostability. We believe that the novel strategy would be a great help to develop more efficient complexes for alternative energy production.

2.5 References

1. L. L. Tinker, N. D. McDaniel, S. Bernhard, *J. Mater. Chem.* **2009**, *19*, 3328.

2. D. Streich, Y. Astuti, M. Orlandi, L. Schwartz, R. Lomoth, L. Hammarstrom, S. Ott, *Chem. Eur. J.* **2010**, *16*, 60.

3. P. Wang, C. Klein, R. Humphry-Baker, S. M. Zakeeruddin, M. Gratzel. *J. Am. Chem. Soc.* **2005**, *127*, 808.

4. D. Kuang, S. Ito, B. Wenger, C. Klein, J. Moser, R. Humphry-Baker, S. M. Zakeeruddin, M. Gratzel, *J. Am. Chem. Soc.* **2006**, *128*, 4146.

5. F. gao, Y. Wang, D. Shi, J. Zhang, M. Wang, X. Jing, R. Humphry-Baker, P. Wang, S. M. Zakeeruddin, M. Gratzel, *J. Am. Chem. Soc*. **2008**, *130*, 10720.

6. F. Gao, Y. Wang, Z. Zhang, D. Shi, M. Wang, R. Humphry-Baker, P. Wang, S. M. Zakeeruddin, M. Gratzel. *Chem. Commun*. **2008**, *23*, 2635.

7. C. –Y. Chen, M. Wang, J. –Y. Li, N. Pootrakulchote, L. Alibabaei, C. Ngocle, J. –D. Decoppet, J. –H. Tsai, C. Gratzel, C. –G. Wu, S. M. Zakeeruddin, M. Gratzel, *ACS Nano*. **2009**, *3*, 3103.

8. K. Cao, J. Lu, J. Cui, Y. Shen, W. Chen, G. Alemu, Z. Wang, H. Yuan, J. Xu, M. Wang, Y. Cheng, *J. Mater. Chem. A.* **2014**, *2*, 4945.

9. C, -Y. Chen, N. Pootrakuchote, S. –J. Wu, M. Wang, J, -Y. Li, J. –H. Tsai, C, -G. Wu, S. M. Zakeeruddin, M. Grätzel, *J. Phys. Chem. C*. **2009**, *113*, 20752

10. J. –H. Yum, I. Jung, C. Baik, J. Ko, M. K. Nazeeruddin, M. Grätzel, *Energy Environ. Sci.* **2009**, *2*, 100

11. A. Mahmood, *Solar Energy*. **2016**, *123*, 127

12. R. S. Khnayzer, C. E. McCusker, B. S. Olaiya, F. N. Castellano, *J. Am. Chem. Soc.* **2013**, 135, 14068

13. E. Mejia, S, -P. Luo, M. Karnahl, A. Friedrich, S. Tschierlei, A. –E. Surkus, H. Junge, S. Gladiali, S. Lochbrunner, M. Beller, *Chem. Eur. J.* **2013**, *19*, 15972

14. A. Kaeser, M. Mohankumar, J. Mohanraj, F. Monti, M. Holler, J. –J. Cid, O Moudam, I. Nierengarten, L. Karmazin-Brelot, C. Duhayon, B. Delavaux-Nicot, N. Armaroli, J. –F. Nierengarten, *Inorg. Chem.* **2013**, *52*, 12140

15. A. F. Larsen, T. Ulven, *Org. Lett.* **2011**, *13*, 3546

16. Y. You, C. –G. An, D. –S. Lee, J. –J. Kim, S. Y. Park, *J. Mater. Chem*. **2006**, *16*, 4706

17. S. –P. Luo, E. Mejia, A. Friedrich, A. Pazidis, H. Junge, A. –E. Surkus, R. Jackstell, S. Denurra, S. Gladiali, S. Lochbrunner, M. Beller, *Angew. Chem. Int. Ed.* **2013**, *52*, 419

18. Valco Instruments Co. Inc. Technical support

19. L. L. Tinker, N. D. McDaniel, P. N. Curtin, C. K. Smith, M. J. Ireland, S. Bernhard, *Chem. Eur. J.* **2007**, *13*, 8726

20. D. S. Miller, G. McLendon, *J. Am. Chem. Soc.* **1981**, *103*, 6791

21. M. –H. Tsai, H. –W. Lin, H. –C. Su, T. –H. Ke, C. Wu, F. –C. Fang, Y. –L. Liao, K. –T. Wong, C. –I. Wu, *Adv. Mater*, **2006**, *18*, 1216

22. S. –P. Luo, N. –Y. Chen, Y. –Y. Sun, L. –M. Xia, Z. –C. Wu, H. Junge, M. Beller, Q. –A. Wu, *Dyes and Pigments*, **2016**, *134*, 580

23. S. Fischer, D. Hollmann, S. Tschierlei, M. Karnahl, N. Rockstroh, E. Barsch, P. Schwarzbach, S. –P. Luo, H. Junge, M. Beller, S. Lochbrunner, R. Ludwig, A. Bruckner, *ACS Catal.* **2014**, *4*, 1845

24. A. J. J. Lennox, S. Fischer, M. Jurrat, S. –P. Luo, N. Rockstroh, H. Junge, R. Ludwig, M. Beller, *Chem. Eur. J*. **2016**, *22*, 1233

25. A. A. Vlcek, E. S. Dodsworth, W. J. Pietro, A. B. P. Lever, *Inorg. Chem.* **1995**, *34*, 1906

2.6 Appendix

^{1}H NMR spectra of synthesized materials

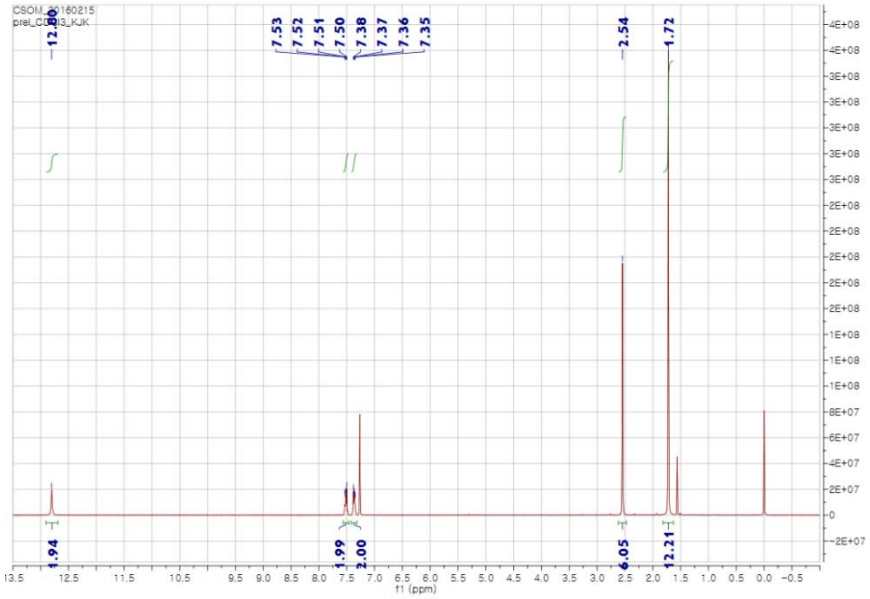

L1 (300 MHz, $CDCl_3$)

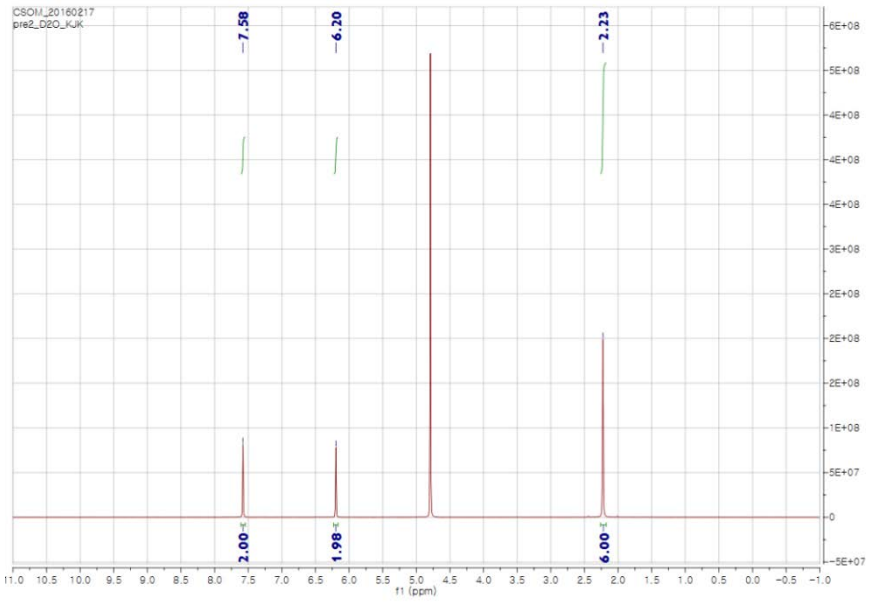

L2 (300 MHz, NaOD in D_2O)

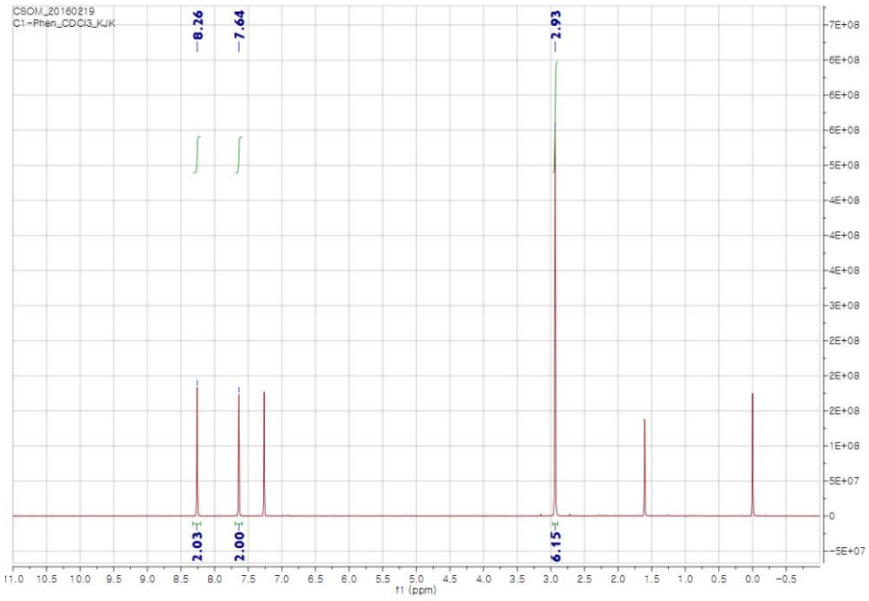

phenCl (300 MHz, $CDCl_3$)

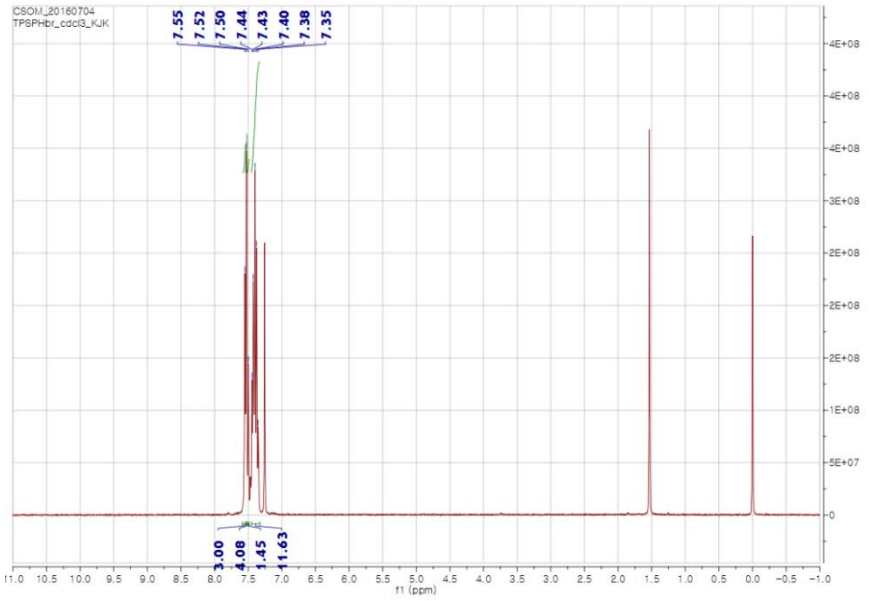

TPSBr (300 MHz, $CDCl_3$)

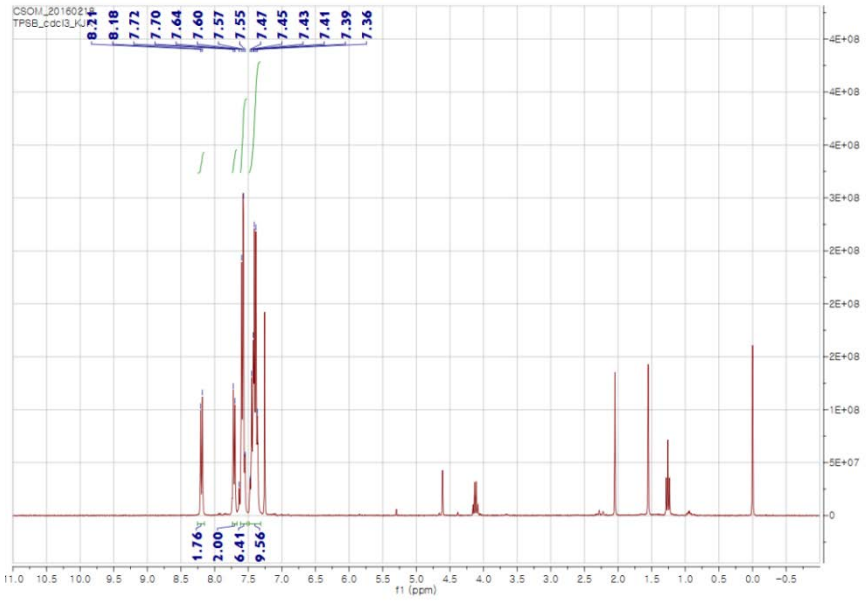

$TPSB(OH)_2$ (300 MHz, $CDCl_3$)

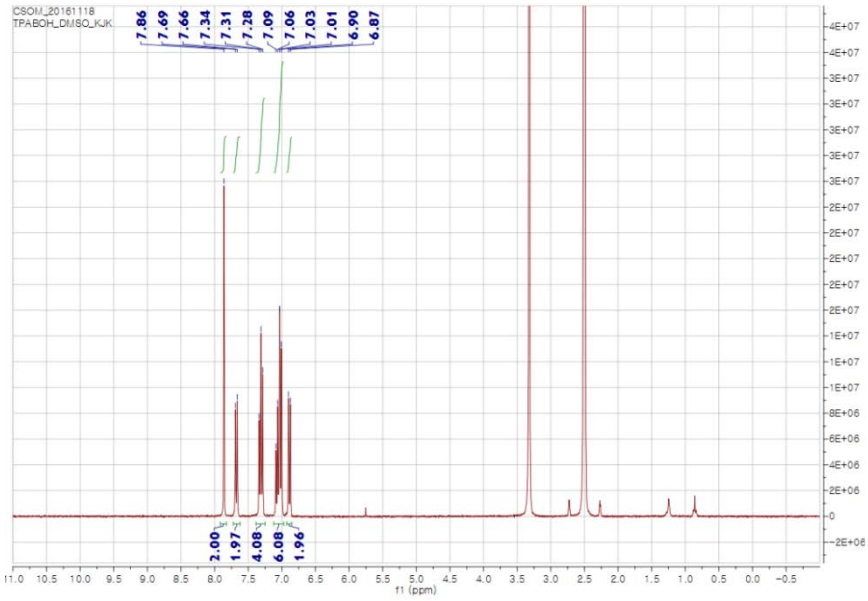

$TPAB(OH)_2$ (300 MHz, DMSO)

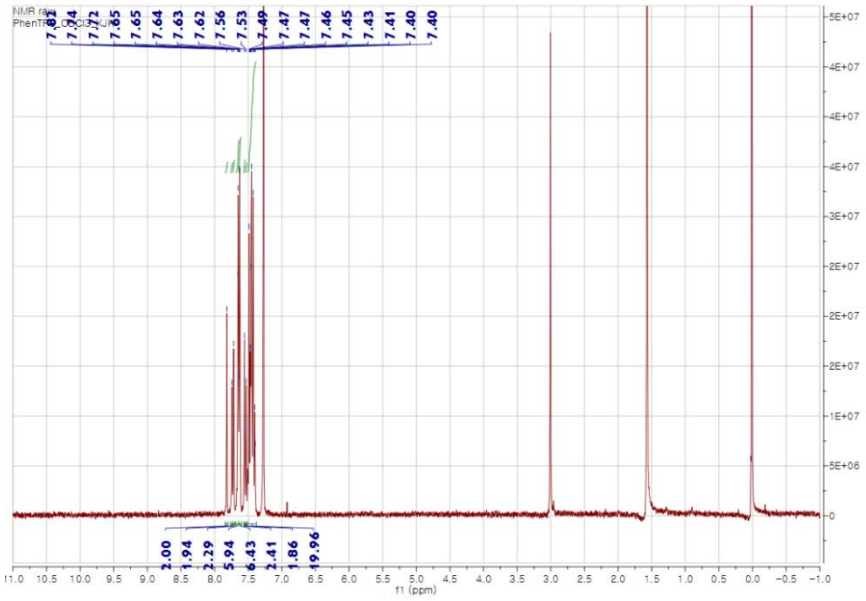

TPSphen (300 MHz, $CDCl_3$)

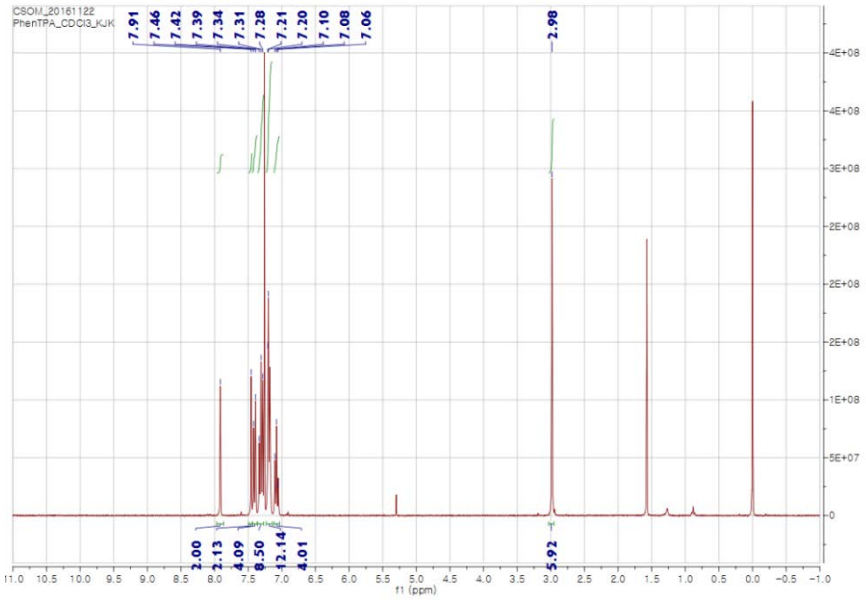

TPAphen (300 MHz, $CDCl_3$)

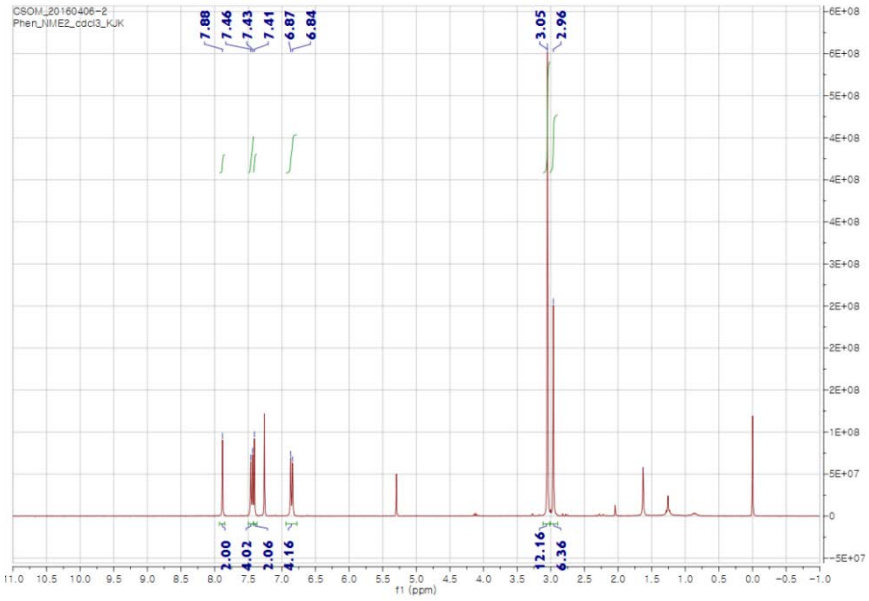

DMAphen (300 MHz, $CDCl_3$)

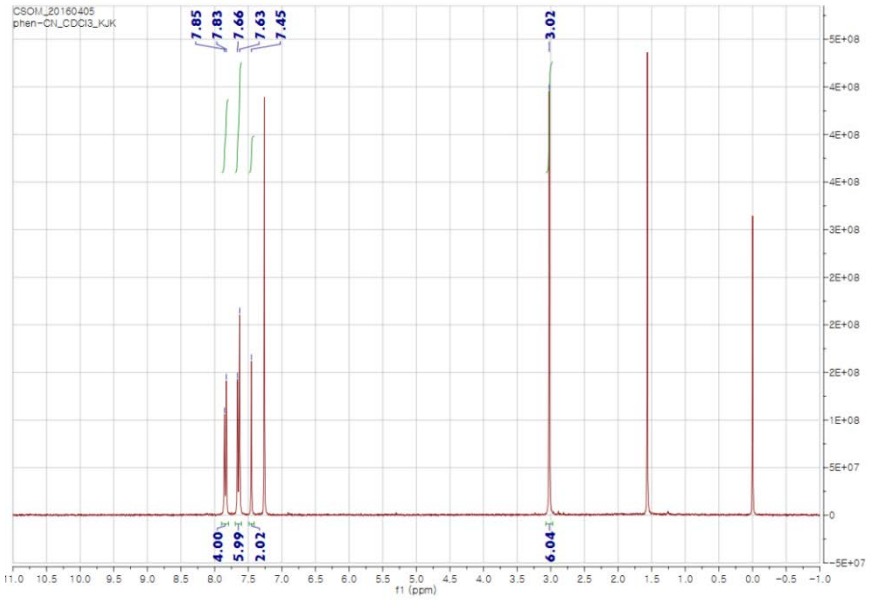

BZNphen (300 MHz, $CDCl_3$)

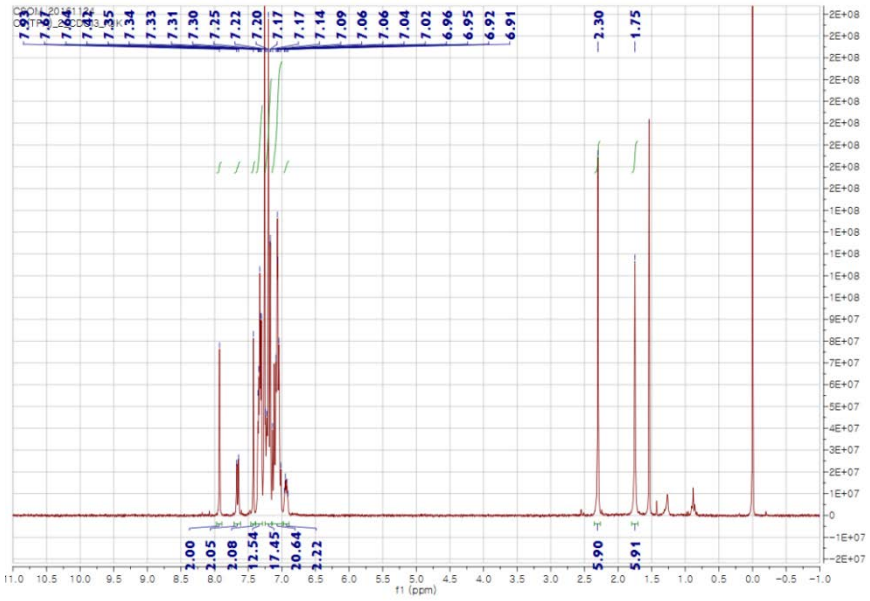

Cu(TPA) (300 MHz, $CDCl_3$)

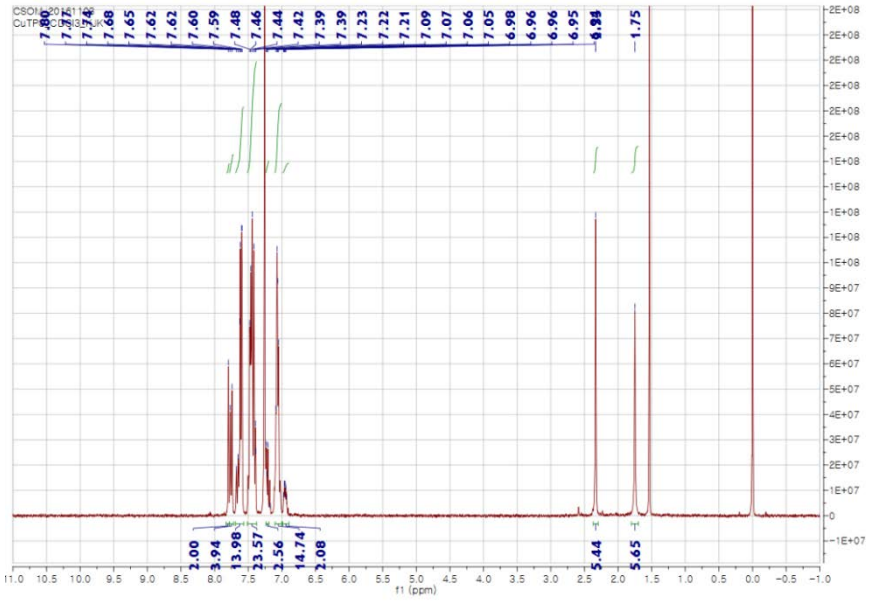

Cu(TPS) (300 MHz, $CDCl_3$)

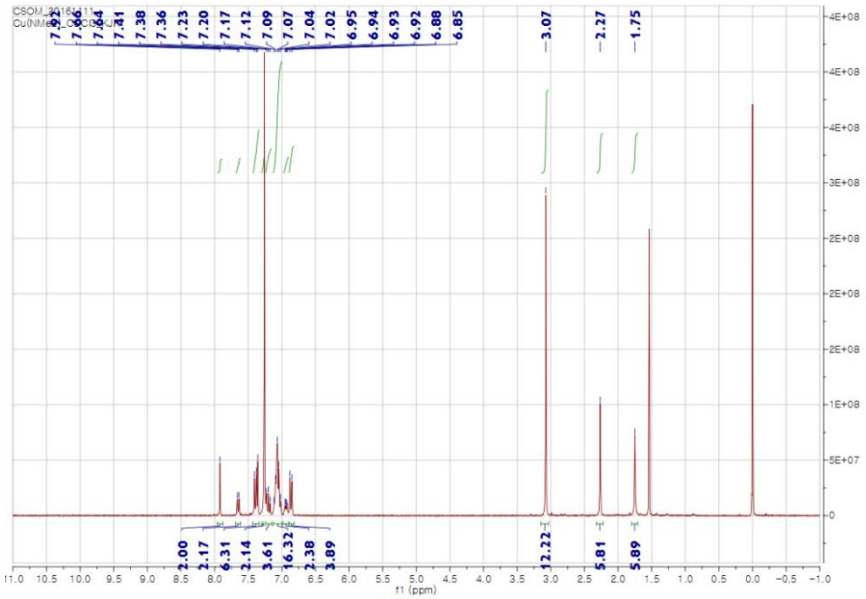

Cu(DMA) (300 MHz, $CDCl_3$)

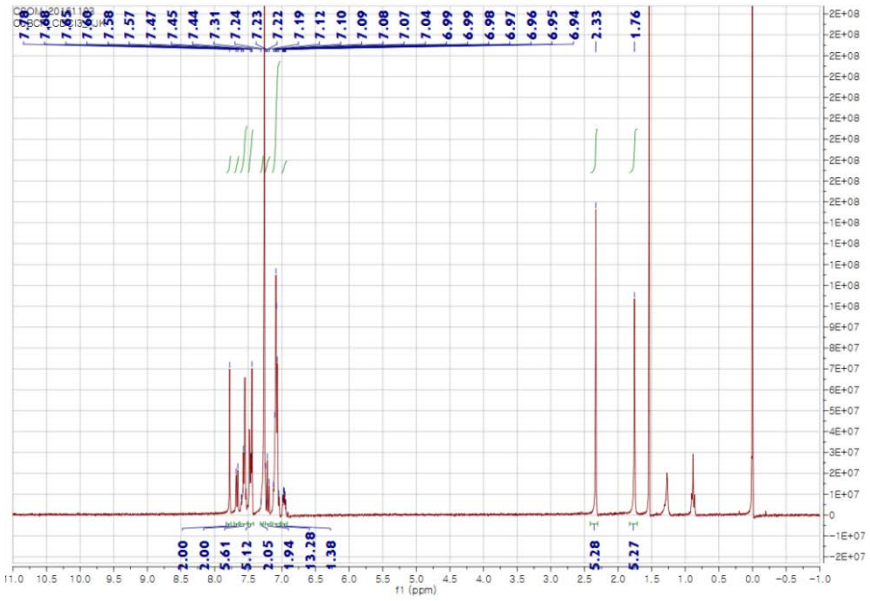

Cu(BCP) (300 MHz, $CDCl_3$)

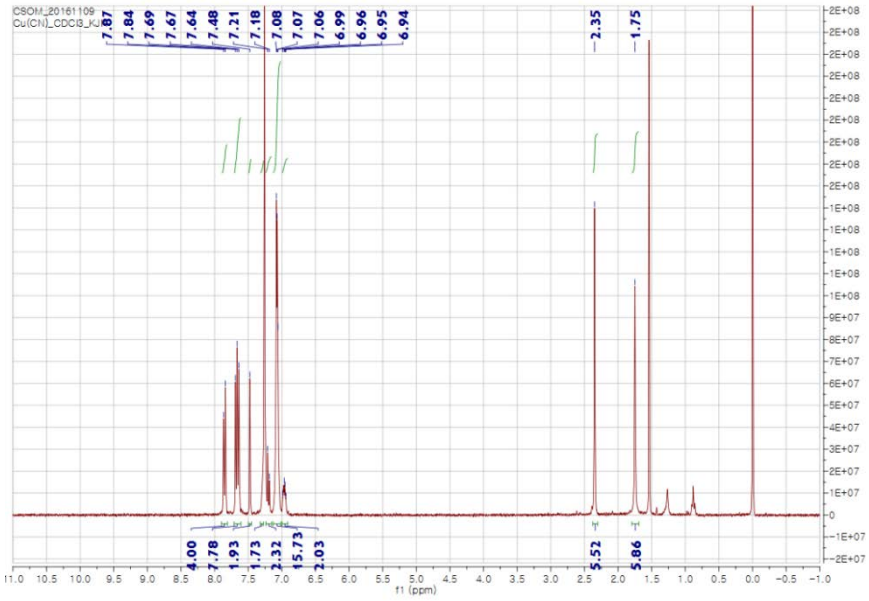

Cu(BZN) (300 MHz, $CDCl_3$)

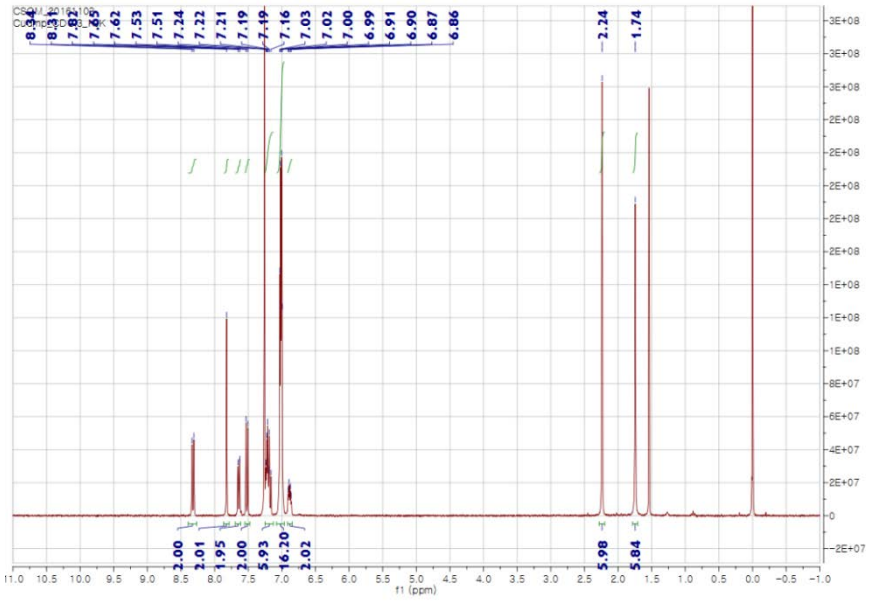

Cu(dmphen) (300 MHz, $CDCl_3$)

^{13}C NMR spectra of synthesized materials

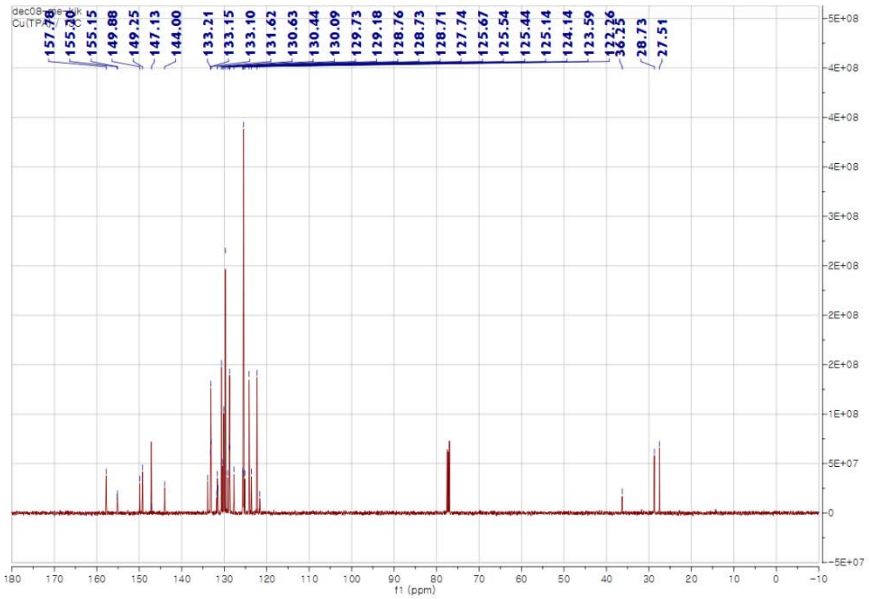

Cu(TPA) (500 MHz, $CDCl_3$)

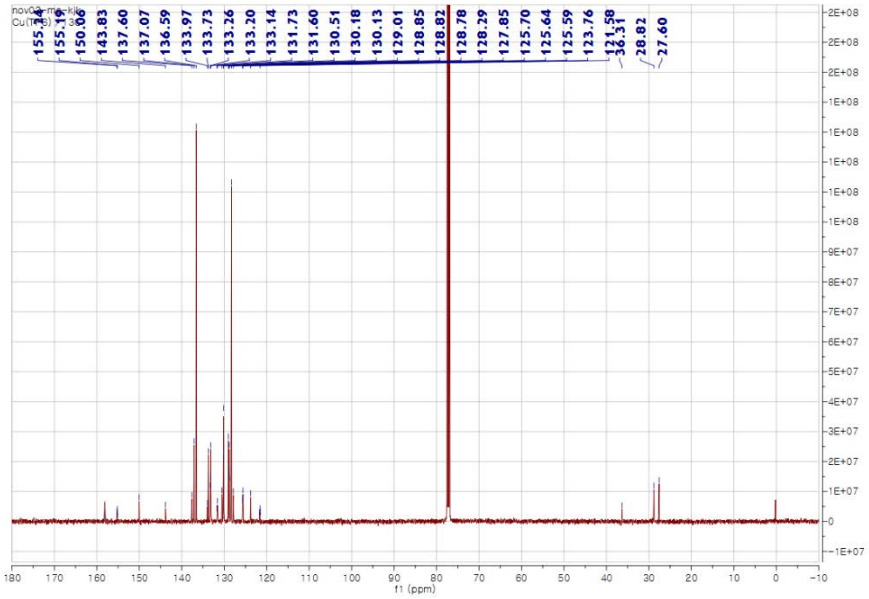

Cu(TPS) (500 MHz, $CDCl_3$)

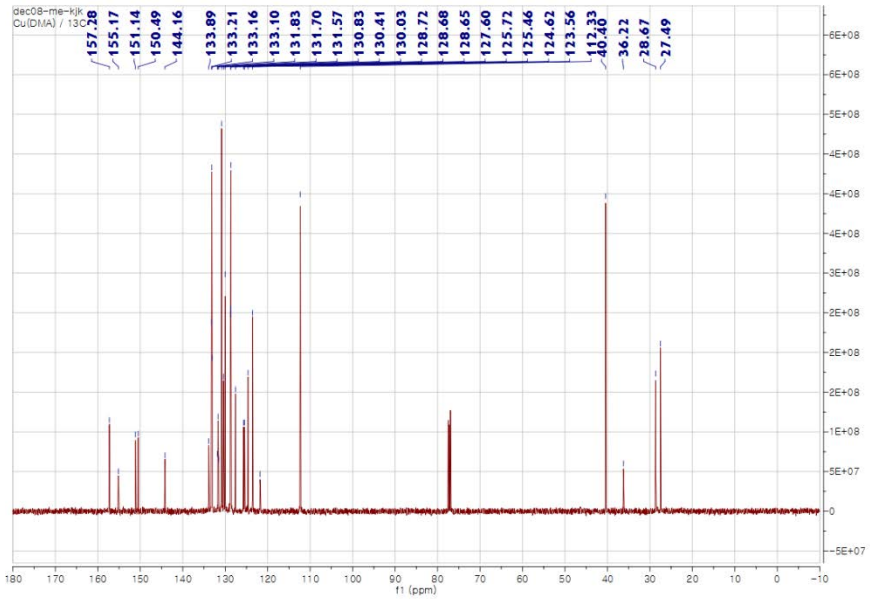

Cu(DMA) (500 MHz, $CDCl_3$)

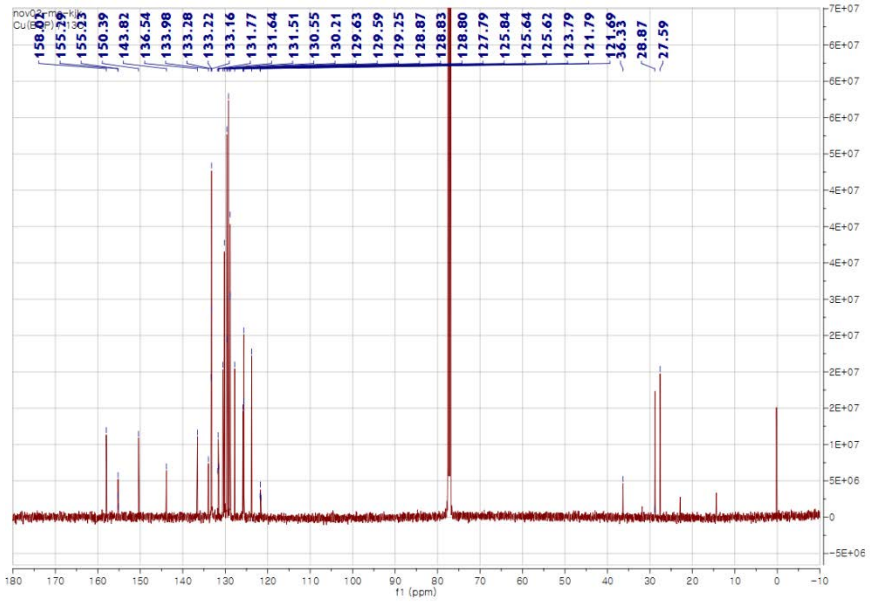

Cu(BCP) (500 MHz, $CDCl_3$)

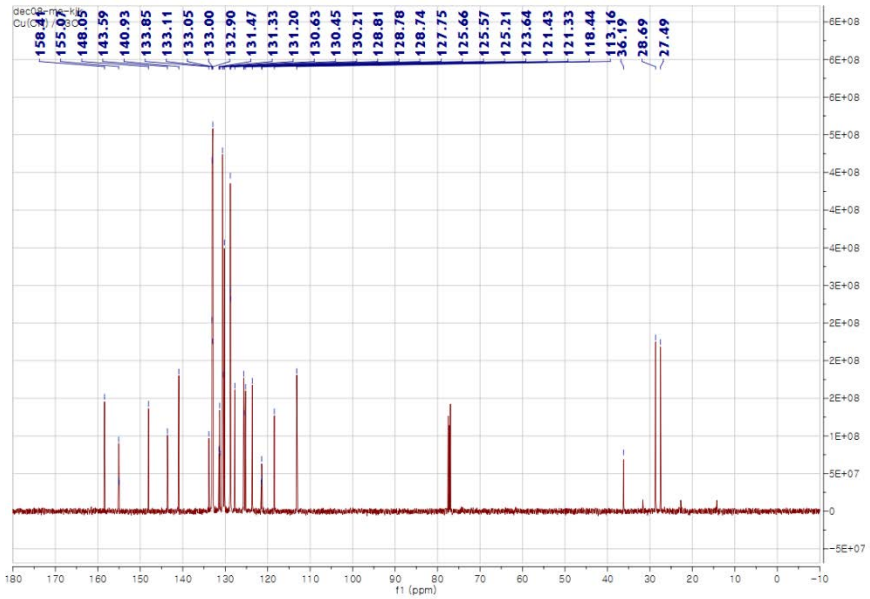

Cu(BZN) (500 MHz, $CDCl_3$)

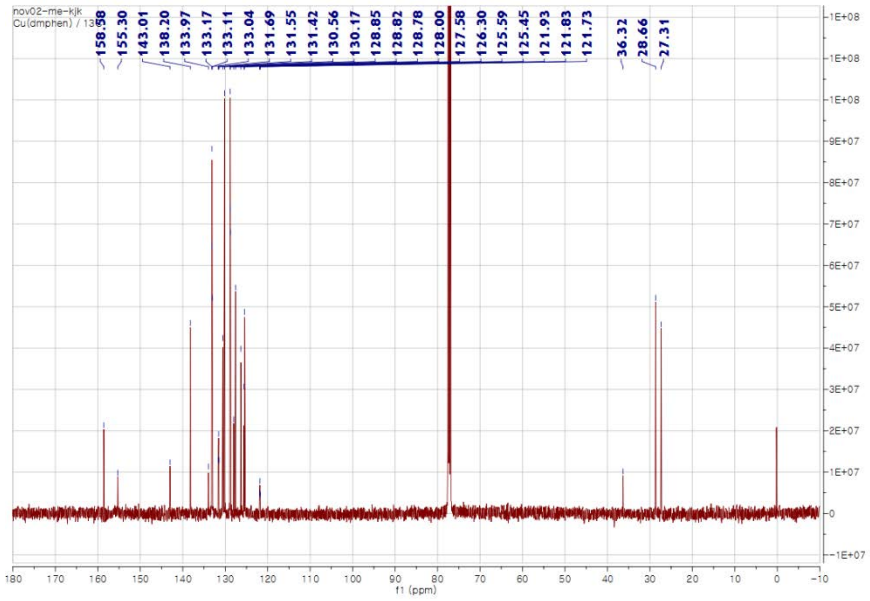

Cu(dmphen) (500 MHz, $CDCl_3$)

초 록

광촉매 물분해 수소생산을 위한 효율적인 구리 기반의 감광제에 대한 연구

현재 인구의 증가과 산업화에 따라 에너지의 수요가 급증하고 있다. 주 에너지원으로 쓰이는 화석연료는 고갈자원이고, 원자력 에너지 등은 그 자체의 위험성에 대한 논란이 아직도 많다. 그리하여 안전하고 친환경적이면서 부족한 자원을 대체할 수 있는 에너지에 대한 인류의 관심이 높아지고 있다. 다양한 대체 에너지 후보 중 수소 에너지는 부산물이 오직 물이라는 점에서 친환경적이고 가볍기 때문에 에너지 밀도가 상당히 높다는 장점이 있다.

이러한 수소를 생산하기 위해 다양한 항법이 있다. 그 중에서 화석연료를 개질하는 것이 현재 대부분이고 물을 전기분해하는 방법도 있다. 하지만 그들은 여전히 환경오염에 대한 문제와 추가의 에너지를 필요로 한다는 단점이 있다. 그리하여 무한한 자원인 태양에너지와 물을 이용한 인공 광합성이 최근 활발히 연구되고 있다.

본 논문에서는 수소를 생산하기 위하여 광촉매 물분해 시스템을 활용하기로 하였다. 광촉매 작용을 일으키기 위해서는 빛을 흡수하여 화학 에너지로 전환해주는 감광제가 필요하다. 감광제로

많이 쓰이는 물질은 루테늄 혹은 이리듐과 같은 귀금속을 이용한 금속착물들이 있다. 이러한 금속 착물들은 가시광선을 흡수할 수 있고 효율적이고 안정하다는 장점이 있지만 실용적인 관점에서 보았을 때 적합하지 않다는 단점이 있다. 그러므로 이러한 귀금속 기반의 금속착물을 값싼 금속을 이용한 착물로 대체하는 것이 필요하다.

그리하여 본 2단원에서는 값싼 금속인 구리를 이용한 효율적인 감광제를 디자인하고 합성하여 그들의 광물리적 특성을 관찰하였고, 실제로 수소생산에 적용한 연구를 보고하였다. 구리 감광제의 수소 생산에 대한 성능이 리간드의 작용기에 의해 어떻게 바뀌는지 알아보기 위하여 다양한 작용기의 구분을 크기와 전자적 성질로 나누어 착물의 성질을 미세 조정하였다. 그 중에서 부피가 크고 전자 주개의 성질을 갖는 triphenylamine 작용기가 붙은 구리 기반 감광제(Cu(TPA))는 리간드 내에 전자 주개가 있어서 금속-리간드 전하이동(MLCT) 뿐 아니라 리간드 내 전하이동(ILCT)가 함께 일어나 가시광선 영역의 빛을 많이 흡수 할 수 있었다. 그 뿐 아니라 감광제로서 필요로 하는 긴 들뜬상태의 수명, 낮은 비발광 소멸을 갖기 때문에 높은 수소 생산 효율을 가질 수 있었다. 그리고 triphenylamine의 큰 부피 때문에 빛에 대하여 가장 안정한 구조를 유지하였다. 그 결과, 4일 동안 turnover number를 18974를 기록하여 가장 효율적인 수소 생산을 보여주었다. Cu(TPA)는 높은 빛의 흡수와 전자 전달 자유 에너지에 비례하여 수소 생산의 빠른 turnover frequency를 보여주었다.

주요어: 인공광합성, 물분해, 광촉매 수소생산, 금속 착물, 구리 기반 감광제
학 번: 2015-20811